Genomic novelty and process-level convergence in adaptation to whole genome duplication

Magdalena Bohutínská[1,2], Mark Alston[3], Patrick Monnahan[3], Terezie Mandáková[4], Sian Bray[3], Pirita Paajanen[3], Filip Kolář[1,2,5], and Levi Yant[6]*

1. Department of Botany, Faculty of Science, Charles University, Prague, Czech Republic
2. Institute of Botany, The Czech Academy of Sciences, Průhonice, Czech Republic
3. Department of Cell and Developmental Biology, John Innes Centre, Norwich Research Park, Norwich, UK
4. CEITEC – Central European Institute of Technology, and Faculty of Science, Masaryk University, Kamenice, Czech Republic
5. Natural History Museum, University of Oslo, Oslo, Norway
6. Future Food Beacon and School of Life Sciences University of Nottingham, Nottingham, UK

Magdalena Bohutínská and Mark Alston contributed equally.

***Author for correspondence:** Levi Yant

Email: levi.yant@nottingham.ac.uk

ORCID: 0000-0003-3442-0217

Classification

BIOLOGICAL SCIENCES: Evolution

Keywords

polyploidy; convergence; evolution; population genomics; genome duplication; adaptation

This PDF file includes:

Main Text
Figures 1 to 4
Tables 1 to 3
SI Appendix

Abstract

Whole genome duplication (WGD) occurs across kingdoms and can promote adaptation. However, a sudden increase in chromosome number, as well as changes in physiology, are traumatic to conserved processes. Previous work in *Arabidopsis arenosa* revealed a coordinated genomic response to WGD, involving physically interacting meiosis proteins, as well as changes related to cell cycle and ion homeostasis. Here we ask: is this coordinated shift in the same processes repeated in another species following WGD? To answer this, we resequenced and cytologically assessed replicated populations from a diploid/autotetraploid system, *Cardamine amara,* and test the hypothesis that gene and process-level convergence will be prevalent between these two WGDs adaptation events. Interestingly, we find that gene-level convergence is negligible, with no more in common than would be expected by chance. This was most clear at meiosis-related genes, consistent with our cytological assessment of somewhat lower meiotic stability in *C. amara*, despite establishment and broad occurrence of the autotetraploid in nature. In contrast, obvious convergence at the level of functional processes, including meiotic cell cycle, chromosome organisation and stress signalling was evident. This indicates that the two autotetraploids survived challenges attendant to WGD via contrasting solutions, modifying different players from similar processes. Overall, this work gives the first insight into the salient adaptations required to cope with a genome-doubled state and brings the first genomic evidence that autopolyploids can utilize multiple trajectories to achieve adaptation to WGD. We speculate that this flexibility increases the likelihood a nascent polyploid overcomes early stringent challenges to later access the spectrum of evolutionary opportunities of polyploidy.

Significance statement

Whole genome duplication (WGD) is a tremendous mutation and an important evolutionary force. It also presents immediate changes to meiosis and cell physiology that nascent polyploids must overcome to survive. Given the dual facts that WGD adaptation is difficult, but many lineages nevertheless survive WGD, we ask: how constrained are the evolutionary responses to a genome-doubled state? We previously identified candidate genes for WGD adaptation in *Arabidopsis arenosa*, which has natural diploid and tetraploid variants. Here we test for evolutionary convergence in adaptation to WGD in a species 17 million years distant, *Cardamine amara*. This work gives the first genomic insight into of how autopolyploids utilize multiple adaptive trajectories to manage a genome-doubled state.

Introduction

Whole genome duplication (WGD) is both a massive mutation and a powerful force in evolution (1). The opportunities and challenges presented by WGD occur immediately, realised in a single generation. As such, WGD comes as a shock to the system. Autopolyploids, formed by within-species WGD (without hybridization), emerge from the chance encounter of unreduced gametes. Thus, they typically harbour four full haploid genomes that are similar in all pairwise combinations, resulting in a lack of pairing partner preferences at meiosis. This, combined with multiple crossover events per chromosome pair, can result in entanglements among three or more homologs at anaphase and mis-segregation or chromosome breakage, leading to aneuploidy (2–4). Beyond this, WGD presents a suddenly transformed intracellular landscape to the conserved workings of the cell, such as altered ion homeostasis and a host of nucleotypic factors related to cell size, volume, and cell cycle progression (3, 5, 6). Occasionally however, a lineage survives this early trauma and graduates to runaway evolutionary success. Indeed, there is some direct empirical evidence of the increased adaptability of autopolyploid lineages from *in vitro* evolutionary competition experiments (7). With increased ploidy, genetic variability can be maintained in a masked state, with evidence of lineages acting as allelic sponges recruiting diverse alleles by gene flow across ploidies, and indeed, species (8, 9). Thus, while substantial opportunities await lineages that adapt to WGD, clear challenges must be overcome to function as a polyploid (3, 10, 11).

The genomic basis for adaptation to WGD has been most extensively investigated in *Arabidopsis arenosa*, which exists as both diploid and autotetraploid in the wild (12). There, the strongest genomic signals of adaptation to WGD are in a suite of 8 genes that cooperatively govern early events in the formation of meiotic chromosome crossovers (13, 14). The products of these genes physically and functionally interact to control this coordinated, conserved process, which stands as a leading candidate process mediating adaptation to WGD. In the evolved *A. arenosa* autotetraploids harbouring these selected alleles, we observed a decrease in meiotic crossover number as well as fewer chromosome entanglements relative to synthetic autopolyploids with ancestral diploid alleles (14). Recent work found that the sister species *Arabidopsis lyrata,* a younger autotetraploid, also harbours many of the same selected alleles discovered in *A. arenosa* (9). Moreover, from a joint population genomic analysis of both species across a hybrid zone, clear signals of bidirectional adaptive gene flow

95 emerge exactly at these adaptive alleles between *A. arenosa* and *A. lyrata* (9, 15). Therefore, *A. lyrata*
96 and *A. arenosa* WGD stabilisation events are not independent.
97
98 Here we use an independent system, ~17 million years diverged from both *A. arenosa* and *A. lyrata*
99 (16), to test the hypothesis that this solution of nimble meiosis gene evolution is repeated, and if not,
100 whether changes in other genes from analogous processes are associated with adaptation to WGD.
101 Given the clear results in *A. arenosa* and *A. lyrata*, we hypothesised that the adaptive trajectories which
102 are available to mediate adaptation to a WGD state may be constrained, leading to repeated selection
103 of the same meiosis genes. Such a result would offer a striking case of convergent evolution in core
104 cellular processes. To test this hypothesis, we take advantage of a well-characterised model, *Cardamine*
105 *amara* (Brassicaceae, tribe Cardamineae). A large-scale cytotyping survey and genetic analysis
106 demonstrated an autopolyploid origin of the successful autotetraploid cytotype found in the Eastern
107 and Central Alps (17–20). Importantly, *C. amara* is a perennial herb harbouring a high level of genetic
108 diversity (similar to both *A. arenosa* and *A. lyrata*) and shares a similar distribution range and
109 evolutionary history, with a likely single origin, followed by autotetraploid expansion associated with
110 glacial oscillations (18, 19).
111
112 To test our hypothesis of gene and process-level convergence, we performed genome scans for
113 selection, contrasting natural autotetraploid and diploid populations. We found the strongest selection
114 signals specifically at genes involved in cellular functions central to adaptation to WGD: chromosome
115 remodelling, meiosis, cell cycle regulation, and ion transport. However, the evolutionary response to
116 WGD in *C. amara* is very different to that of *A. arenosa*: overall, we saw minimal gene-level convergence
117 in loci putatively mediating adaptation to WGD. In particular, none of the same meiosis-related genes
118 that control meiotic chromosome crossovers in *A. arenosa* were under selection in *C. amara*. This is
119 consistent with observations of clonal spreading and lower meiotic stability in both diploid and
120 autotetraploid *C. amara*, suggesting that *C. amara* autotetraploids are already prepared by their diploid
121 lifestyle to thrive, at least temporarily, while suffering reduced meiotic fidelity. However, in contrast to
122 a lack of gene convergence, we find a strong signal of process-level convergence in core processes
123 controlling DNA management, chromosome organisation, stress signalling, and ion homeostasis.
124 Overall, our results provide sharp contrast to widespread reports of gene-level convergence across the

tree of life and suggest that the genomic changes associated with a WGD state might not be as constrained as would be expected based on their functional conservation across eukaryotes.

Results and Discussion

Population selection, sampling and genetic structure. To assess the genetic basis of adaptation to WGD in *C. amara*, we generated a novel synthetic long-read reference genome (N50 = 1.82 mb, 95% complete BUSCOs; see Methods) and resequenced in triplicate four populations of contrasting ploidy, sampling 100 individuals: two diploid (LUZ, VRK) and two autotetraploid (CEZ, PIC; Fig. 1A; *SI Appendix*, Table S1). We chose these populations based on a comprehensive cytological survey of over 3,000 *C. amara* samples throughout the Czech Republic (18). The populations we sampled represent core areas of each cytotype, away from potential hybrid zones and distant from any triploid-containing populations. Further, we performed flow cytometry on all samples sequenced to verify expected ploidy.

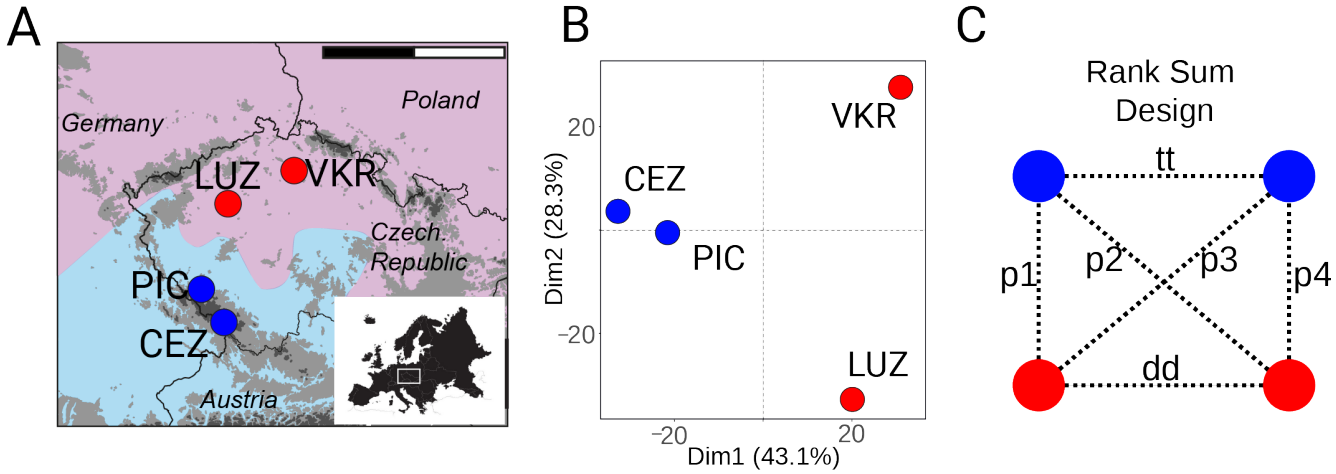

Figure 1. Sample population locations and population structure of *Cardamine amara*. A, Locations of *C. amara* populations sampled in the Czech Republic (red, diploids; blue, autotetraploids; scale bar corresponds to 200 km; shaded area represents each cytotype range from (18), with autotetraploid range expansion southward). **B**, Population structure represented by Principal Component Analysis of ~124,000 fourfold degenerate SNPs. **C**, Rank Sum design used to minimise any influence of population-specific divergence in tests for directional selection. 'p1' to 'p4' represent the between-ploidy contrasts used for the rank sum calculations. 'dd' and 'tt' represent within-ploidy contrasts used to subtract signal of local population history.

To obtain robust population allele frequency estimates across genomes, we performed a replicated pooled sequencing approach. From each population we pooled DNA from 25 individuals in triplicate and generated on average 31 million reads per pooled sample. We mapped the reads onto our *C. amara*

149 assembly. After read mapping, variant calling and quality filtration, we obtained a final dataset of
150 2,477,517 SNPs (mean coverage depth per population = 86, *SI Appendix*, Table S2).
151
152 Population structure of *C. amara* (Fig. 1B) showed primary differentiation by ploidy (first axis explained
153 43% of all variability) while the second axis (28% of variability explained) differentiated the two diploid
154 populations from each other. The two autotetraploid populations had the lowest genetic differentiation
155 of all contrasts (Fst = 0.04, mean allele frequency difference = 0.06) and showed a complete absence of
156 fixed differences (Table 1). Close genetic similarity together with spatial arrangement (the populations
157 represent part of a continuous range of autotetraploid cytotype spanning to Eastern Alps) suggest that
158 both autotetraploid populations represent the outcome of a single polyploidization event, in line with
159 previous population genetic inference based on large-scale sampling (18). The similar level of
160 interploidy divergence within both *C. amara* and *A. arenosa* (average Fst between diploids and
161 autotetraploids = 0.10 and 0.11, respectively) suggests that the polyploidization events in both species
162 happened at roughly comparable time points in the past (Table 1).
163
164 **Table 1.** Measures of genome-wide differentiation between *C. amara* and *A. arenosa* populations

Populations	Ploidies	AFD	Fixed diff	Fst	# SNPs
PIC - VKR	4x - 2x	0.09	30	0.09	2,326,315
PIC - LUZ	4x - 2x	0.09	2	0.08	2,314,229
CEZ - VKR	4x - 2x	0.11	120	0.12	2,333,538
CEZ - LUZ	4x - 2x	0.11	86	0.11	2,335,004
CEZ - PIC	4x - 4x	0.06	0	0.04	2,297,229
LUZ - VKR	2x - 2x	0.1	6	0.09	2,018,892
A. arenosa tetraploids - *A. arenosa* diploids	4x - 2x	0.05	21	0.11	7,106,848

165 **Note:** Differentiation metrics shown are mean allele frequency difference (AFD), the number of fixed differences
166 (Fixed diff) and Fst. In the case of *A. arenosa,* Fst in diploids is calculated as a mean over all pairwise Fst
167 measurements between the five previously characterised diploid lineages (8).
168
169 **Directional selection specifically associated with WGD in *C. amara.*** To minimise false positives due to
170 local population history we leveraged a quartet-based sampling design (21), consisting of two diploid
171 and two autotetraploid populations (Fig. 1C). We calculated Fst for 1 kb windows with a minimum 20
172 SNPs for all six possible population contrasts, and ranked windows based on Fst values. The mean
173 number of SNPs per population contrast was 2,270,868 (Table 1). To focus on WGD-associated

174 adaptation, we first assigned ranks to each window based on the Fst values in each of four possible
175 pairwise diploid-autotetraploid contrasts and identified windows in the top 1% outliers of the resultant
176 combined rank sum (Fig. 1C, contrasts p1-p4). We then excluded any window which was also present
177 in the top 1% Fst outliers in diploid-diploid or autotetraploid-autotetraploid population contrasts to
178 avoid misattribution caused by local population history (Fig. 1C, contrasts' tt' and 'dd'). By this
179 conservative approach, we identified 440 windows that intersected 229 gene coding loci (*SI Appendix*,
180 Table S3; 'WGD adaptation candidates' below). Among these 229 gene coding loci, a Gene Ontology
181 (GO) term enrichment analysis yielded 22 significantly enriched biological processes (Fisher's exact test
182 with conservative 'elim' method, adjusted $p < 0.05$, *SI Appendix*, Table S4). To further refine the gene
183 list to putatively functional candidates we complemented these differentiation measures with a
184 quantitative estimate following the fineMAV method (22) (see Methods). SNPs were assigned a
185 fineMAV score based on the predicted functional consequences of amino acid substitutions, using
186 Grantham scores, amplified by the allele frequency difference between the two amino acids (22). From
187 our 229 Fst WGD adaptation candidates, 120 contained at least one 1% fineMAV outlier amino acid
188 substitution (*SI Appendix*, Table S3, S5).
189
190 **DNA maintenance (repair, chromosome organisation) and meiosis under selection in *C. amara*.** Of
191 the 22 significantly enriched GO processes, the most significantly enriched by far was 'DNA metabolic
192 process' (p-value = 6.50E-08, vs 0.00021 for the next most confident enrichment), although there was
193 also enrichment for 'chromosome organization' and 'meiotic cell cycle.' The 40 genes contributing to
194 these categories have specifically localised peaks of differentiation (Fig. 2), as well as 1% fineMAV
195 outlier SNPs in their gene coding regions (Fig. 2, *SI Appendix*, Table S3). These genes also cluster in
196 STRING interaction networks, suggesting coevolutionary dynamics driving these selection signatures
197 (Figure S1; see Methods and Results below). The largest cluster comprises of *MSH6, PDS5e, SMC2, MS5,*
198 *PKL, HDA18, CRC*, and homologs of two uncharacterised, but putative DNA repair related loci
199 *AT1G52950* and *AT3G02820* (containing SWI3 domain). *MutS Homolog 6* (*MSH6*) is a component of the
200 post-replicative DNA mismatch repair system. It forms a heterodimer with MSH2 which binds to DNA
201 mismatches (23, 24), enhancing mismatch recognition. *MutS* homologs have also been shown to
202 control crossover number in *A. thaliana* (25). The *C. amara* ortholog of *AT1G15940* is a close homolog
203 of *PDS5,* a protein required in fungi and animals for formation of the synaptonemal complex and sister
204 chromatid cohesion (26). *Structural Maintenance Of Chromosomes 2* (*SMC2/TTN3*) is a central

205 component of the condensin complex, which is required for segregation of homologous chromosomes
206 at meiosis (27) and stable mitosis (28). *PICKLE* (*PKL*) is a SWI/SWF nuclear-localized chromatin
207 remodelling factor (29, 30) that also has highly pleiotropic roles in osmotic stress response (31),
208 stomatal aperture (32), root meristem activity (33), and flowering time (34). Beyond this cluster, other
209 related DNA metabolism genes among our top outliers include *DAYSLEEPER* (Fig. 2), a domesticated
210 transposase that is essential for plant development, first isolated as binding the *Kubox1* motif upstream
211 of the DNA repair gene *Ku70* (35). The complex Ku70/Ku80 regulate non-homologous end joining (NHEJ)
212 double-strand break repair (36). Consistent with this, *DAYSLEEPER* mutants accumulate DNA damage
213 (37), but the exact role of *DAYSLEEPER* in normal DNA maintenance is not understood. Interesting also
214 is the identification of *MALE-STERILE 5* (*MS5/TDM1*), which is required for cell cycle exit after meiosis
215 II. As the name implies, MS5 mutants are male sterile, with pollen tetrads undergoing an extra round
216 of division after meiosis II without chromosome replication (38). *MS5/TDM1* may be an APC/C
217 component whose function is to ensure meiosis termination at the end of meiosis II (39). Together, this
218 set of DNA management loci exhibiting the strongest signals of selection points to widespread
219 modulation of DNA repair and chromosome management following WGD in *C. amara.*
220

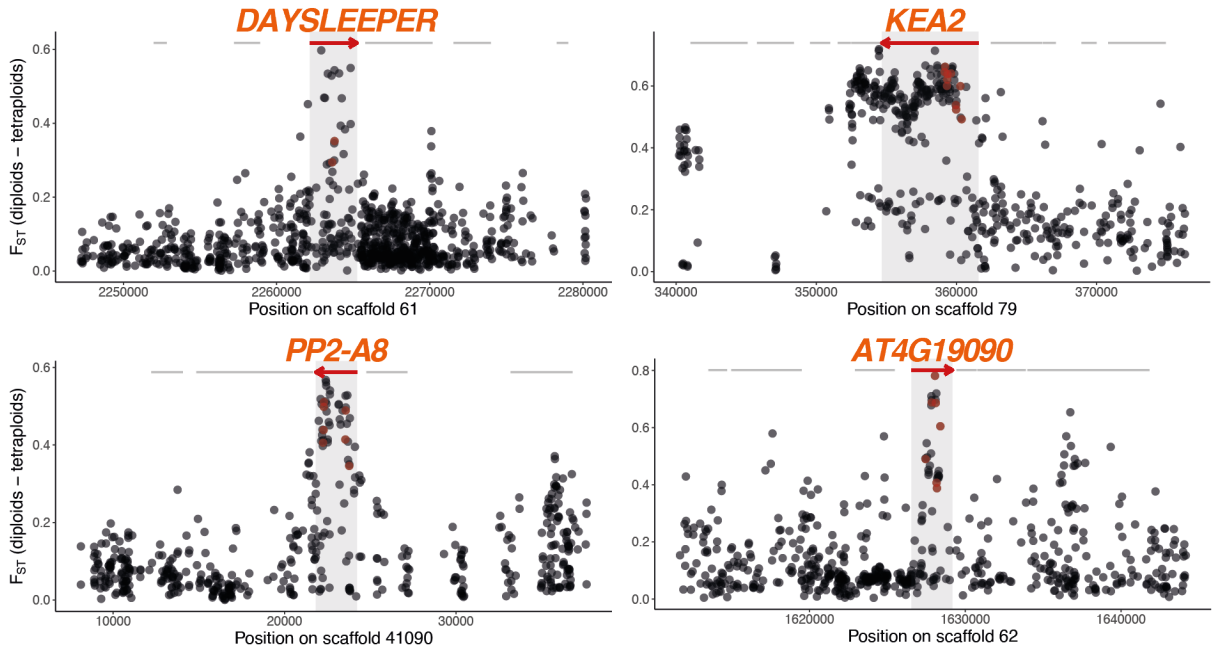

221

222 **Figure 2. Selective sweep signatures at DNA management and ion homeostasis loci.** Examples of selective
223 sweep signatures among four loci (red) among Fst candidate genes. X-axis gives scaffold position in base pairs.
224 Y-axis gives Fst values at single-nucleotide polymorphisms (dots) between diploid and autotetraploid *C. amara*.
225 Red dots indicate fineMAV outlier SNPs. Red arrows indicate gene models overlapping top 1% Fst windows and
226 grey lines indicate neighbouring gene coding loci.

227
228 **Evolution of stress, signalling, and ion homeostasis genes.** The remainder of the enriched GO
229 categories in *C. amara* revolved around a diversity of intracellular processes, including abiotic and biotic
230 stress response, protein phosphorylation, root development, ABA signalling, and ion homeostasis. The
231 intersection of these processes was often represented by several genes. For example, two of the top
232 20 highest-scoring SNPs in the genome-wide fineMAV analysis reside in SNF1-related protein kinase
233 SnRK2.9 (*SI Appendix*, Table S5). SnRKs have been implicated in osmotic stress and root development
234 (40, 41), and their activity also mediates the prominent roles of Clade A protein phosphatase 2C
235 proteins in ABA and stress signalling (42). Interesting in this respect is a strong signature of selection in
236 *HIGHLY ABA-INDUCED PP2C GENE 1,* a clade A *PP2C* protein (*SI Appendix*, Table S3). Stress-related
237 phosphoinositide phosphatases are represented by *SAC9*, mutants of which exhibit constitutive stress
238 responses (43). Diverse other genes related to these categories exhibit the strongest signatures of
239 selection, such as *PP2-A8* (44) and *AT4G19090*, a transmembrane protein strongly expressed in young
240 buds (45) (Fig. 2).
241
242 Given the observed increase in potassium and dehydration stress tolerance in first generation
243 autotetraploid *A. thaliana* (5), it is very interesting that our window-based outliers include an especially
244 dramatic selective sweep at *K^+ Efflux Antiporter 2* (*KEA2*, Fig. 2), a K^+ antiporter that modulates
245 osmoregulation, ion, and pH homeostasis (46). Recent evidence indicates that *KEA2* is important for
246 eliciting a rapid hyperosmotic-induced Ca^{2+} response to water limitation imposed by osmotic stress
247 (47). The *KEA2* locus in autotetraploid *C. amara* features an exceptional ten fineMAV-outlier SNPs (Fig.
248 2, *SI Appendix*, Table S3, S5), indicating that the sweep contains a run of radical amino acid changes at
249 high allele frequency difference between the ploidies, strongly suggesting a ploidy-selected functional
250 change. We also detect *cation-chloride co-transporter 1* (*HAP 5*) a Na+, K+, Cl− co-transporter, involved
251 in diverse developmental processes and Cl− homeostasis (48).
252
253 **Limited gene-level convergence between *C. amara* and *A. arenosa***. We hypothesized that WGD
254 imposed strong, specific selection pressures leading to convergent directional selection on the same
255 genes or at least on different genes playing a role in the same process (gene- or function-level
256 convergence, respectively) between *C. amara* and *A. arenosa*. To test for this, we complemented our
257 *C. amara* genome scan with an analysis of *A. arenosa* divergence outliers based on an expanded

258 sampling relative to the original *A. arenosa* genome scan studies (13, 14). We selected the 80 diploid
259 and 40 autotetraploid individuals sequenced most deeply in a recent range-wide survey (8) of genomic
260 variation in *A. arenosa* (mean coverage depth per individual = 18; 160 haploid genomes sampled of
261 each ploidy), and scanned for Fst outliers in 1 kb windows, as we did for *C. amara*. We identified 696
262 windows among 1% Fst outliers, overlapping 452 gene-coding loci (*SI Appendix*, Table S6), recovering
263 results similar to (14), including the interacting set of 8 loci that govern meiotic chromosome
264 crossovers. However, from this entire list of 452 *A. arenosa* WGD adaptation candidates, only six
265 orthologous loci were shared with our 229 *C. amara* WGD adaptation candidates (Table 2). This degree
266 of overlap was not significant (p = 0.42, Fisher's exact test), indicating no excess convergence at the
267 level of orthologous genes beyond random overlap. Similarly, there was no excess overlap among genes
268 which harbour at least one candidate fineMAV substitution (3 overlapping candidate genes out of 120
269 in *C. amara* and 303 in *A. arenosa*; p = 0.27, Fisher's exact test). This lack of convergence at the ortholog
270 level may come as a surprise given the expected shared physiological challenges attendant to WGD (3).
271

272 **Table 2.** WGD adaptation candidates in both *A. arenosa* and *C. amara.*

C. amara ID	A. thaliana ID	A. arenosa ID	Name	Function (TAIR)
CAg1480	*AT1G16460*	*AL1G28600*	MST2/RDH2	embryo/seed development
CAg20214	***AT2G45120***	***AL4G44210***	**C2H2-like zinc finger**	**stress response**
CAg11103	***AT3G42170***	***AL3G27110***	**DAYSLEEPER**	**DNA repair**
CAg16465	*AT3G62850*	*AL1G11960*	zinc finger-like	unknown
CAg4024	***AT5G05480***	***AL6G15370***	**Asparagine amidase A**	**growth and development**
CAg5641	*AT5G23570*	*AL6G34840*	SGS3	posttranscriptional gene silencing

273 **Note:** The number of genes does not exceed random expectations for the overlap of candidate gene lists from
274 each species, indicating a lack of gene-level convergence. Genes in bold also harbour at least one candidate
275 fineMAV SNP in both species.

276

277 To determine whether we may have failed to detect convergent loci due to missing data or if genes that
278 stand as top outliers in *A. arenosa* had few, but potentially functionally-implicated, differentiated SNPs
279 in *C. amara*, we performed a targeted search in *C. amara* for the interacting set of meiosis proteins
280 found to exhibit the most robust signatures of selection in *A. arenosa* (14). All meiosis-related orthologs
281 in *C. amara* that also exhibit selection signatures in *A. arenosa* (13 in total) passed our data quality
282 criteria and were included in our analyses. Three showed any signal at all by fineMAV analysis: *PDS5b*
283 harbours an unusually high three fineMAV outlier SNPs, although it is not a window based Fst outlier.

284 *ASY3*, which controls crossover distribution at meiosis, has only one fineMAV 1% outlier polymorphism.
285 **Error! Bookmark not defined.**Finally, a regulator of endoreduplication, *CYCA2;3*, also harbours a
286 single fineMAV 1% outlier SNP in *C. amara*, although it was not included in the Fst window analysis
287 (number of SNPs < 20). However, upon inspection of Fst values of the (unusually low) 7 SNPs in the
288 window overlapping this gene, the selection signal in CYCA2;3 would be high (mean Fst = 0.55). Thus,
289 while we detect varying signal in these three meiosis-related genes following WGD, we do not see
290 signals of selection in the conspicuous set of interacting crossover-controlling genes that were obvious
291 in *A. arenosa* (14).
292
293 **Meiotic stability in *C. amara.*** Despite our broad overall analysis of selection in *C. amara*, as well as a
294 targeted assessment of the particular meiosis genes, we did not detect a signal of selection in those
295 genes in *C. amara* (*SI Appendix*, Table S8). The *C. amara* autotetraploid is well-established lineage that
296 underwent significant niche expansion in nature (18), but we still wondered if a contrast in meiotic
297 behaviour underlies this difference in specific loci under selection. Therefore, we cytologically assessed
298 the degree of male meiotic stability in *C. amara* (Fig. 3A). This revealed a low degree of stability in both
299 *C. amara* cytotypes (mean proportion stable metaphase I cells in diploid maternal seed lines = 0.38 –
300 0.69, n = 133 scored cells; in tetraploids = 0.03 – 0.38; n = 348 scored cells; *SI Appendix*, Table S9).
301 However, the degree of meiotic stability was lower in autotetraploids compared to diploids (differing
302 proportion of stable to unstable meiotic cells for each ploidy; D = 62.7, df = 1, p < 0.0001, GLM with
303 binomial errors; Fig. 3B, *SI Appendix*, Table S9), which corresponds with the lack of selection signal in
304 crossover-controlling meiosis genes. Interestingly, we did find that the degree of stability was variable
305 within each cytotype, suggesting the existence of standing genetic variation that controls stability. In
306 contrast, higher frequencies of stable metaphase I cells (>80%) have been observed for diploid and
307 autotetraploid *A. arenosa* (9). This, together with the observation of frequent clonal spreading of *C.*
308 *amara* (49), indicates that the species has an ability to maintain stable populations, even under varying
309 efficiencies of euploid gamete production, thus perhaps decreasing the urgency to fully stabilise meiosis
310 in either cytotype. This, in turn, may have facilitated the establishment of the autotetraploid cytotype.

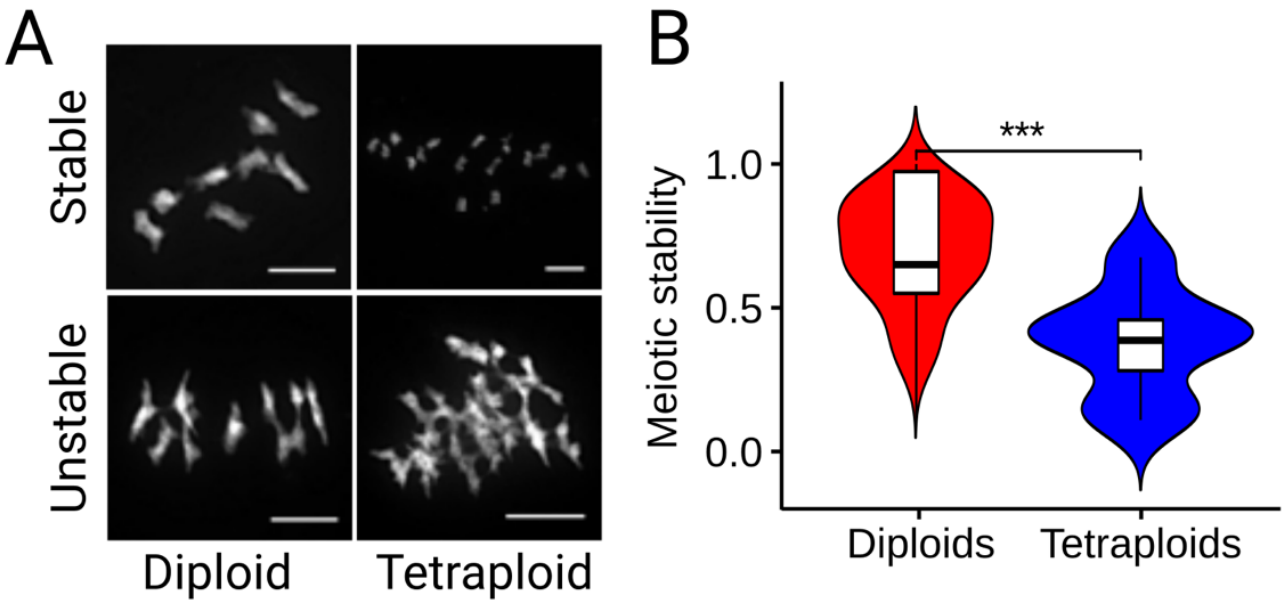

Figure 3. Variable meiotic stability in *C. amara*. A, An example of stable and unstable diploid (8 bivalents) and autotetraploid (16 bivalents) DAPI-stained meiotic chromosomes (diakinesis and metaphase I). Unstable meiosis is characterised by multivalent formation and interchromosomal connections. Scale bar corresponds to 10 µm. For a complete overview of all scored chromosome spreads see Figure S4. **B,** Distribution of meiotic stability (calculated as proportion of stable and partly stable to all scored meiotic spreads) in diploid and autotetraploid individuals of *C. amara.* *** - $p < 0.001$, GLM with binomial errors.

Evidence for process-level convergence. While we found no excess convergence at the level of orthologous genes under selection, we speculated that convergence may occur nevertheless at the level of functional processes. To test this, we used two complementary approaches: overlap of GO term enrichment and evidence of shared protein function from interaction networks. First, of the 73 significantly ($p < 0.05$) enriched GO terms in *A. arenosa* (*SI Appendix*, Table S7), we found that five were identical to those significantly enriched in *C. amara*, which is more than expected by chance ($p < 0.001$, Fisher's exact test; Table 3). In addition, some processes were found in both species, but were represented by slightly different terms, especially in the case of meiosis ("meiotic cell cycle" in *C. amara*, "meiotic cell cycle process" in *A. arenosa*: Tables S4 and S7). Remarkably, the relative ranking of enrichments of all five convergent terms was identical in both *C. amara* and *A. arenosa* (Table 3). This stands in strong contrast to the fact that *A. arenosa* presented an obvious set of physically and functionally interacting genes in the top two categories ('DNA metabolic process' and 'chromosome organisation'), while the genes in these categories in *C. amara* are implicated in more diverse DNA management roles.

334

335 **Table 3.** Convergent processes under selection in both *C. amara* and *A. arenosa* following WGD

GO ID	Term	p-value (*C. amara*)	p-value (*A. arenosa*)	Enrichment (*C. amara*)	Enrichment (*A. arenosa*)
GO:0006259	DNA metabolic process	6.50E-08	8.20E-04	3.72	2.46
GO:0051276	chromosome organization	0.019	2.10E-04	1.98	2.01
GO:0009738	abscisic acid-activated signalling pathway	0.032	0.022	2.54	2.10
GO:0071215	cellular response to abscisic acid stimulation	0.048	0.04	2.30	1.90
GO:0097306	cellular response to alcohol	0.048	0.04	2.30	1.90

336 **Note:** p-values given are Fisher's exact test using the conservative 'elim' method, which tests for enrichment of
337 terms from the bottom of the GO hierarchy to the top and discards any genes that are significantly enriched in a
338 descendant GO terms (Methods). 'Enrichment' refers to fold enrichment.

339

340 Second, we sought for evidence that genes under selection in *C. amara* might interact with those found
341 under selection in *A. arenosa*, which would further support process-level convergence between the
342 species. Thus, we took advantage of protein interaction information from the STRING database, which
343 provides an estimate of proteins' joint contributions to a shared function (50). For each *C. amara* WGD
344 adaptation candidate we searched for the presence of STRING interactors among the *A. arenosa* WGD
345 adaptation candidates, reasoning that finding such an association between candidates in two species
346 may suggest that directional selection has targeted the same processes in both species through
347 different genes. Following this approach, we found that out of the 229 *C. amara* WGD adaptation
348 candidates, 90 were predicted to interact with at least one of the 452 WGD adaptation candidates in
349 *A. arenosa*. In fact, 57 likely interacted with more than one *A. arenosa* candidate protein (Fig. 4 and *SI*
350 *Appendix*, Table S10). This level of overlap was greater than expected by chance (p = 0.001 for both
351 "any interaction" and "more-than-one interaction", as determined by permutation tests with the same
352 database and 1000 randomly generated candidate lists).

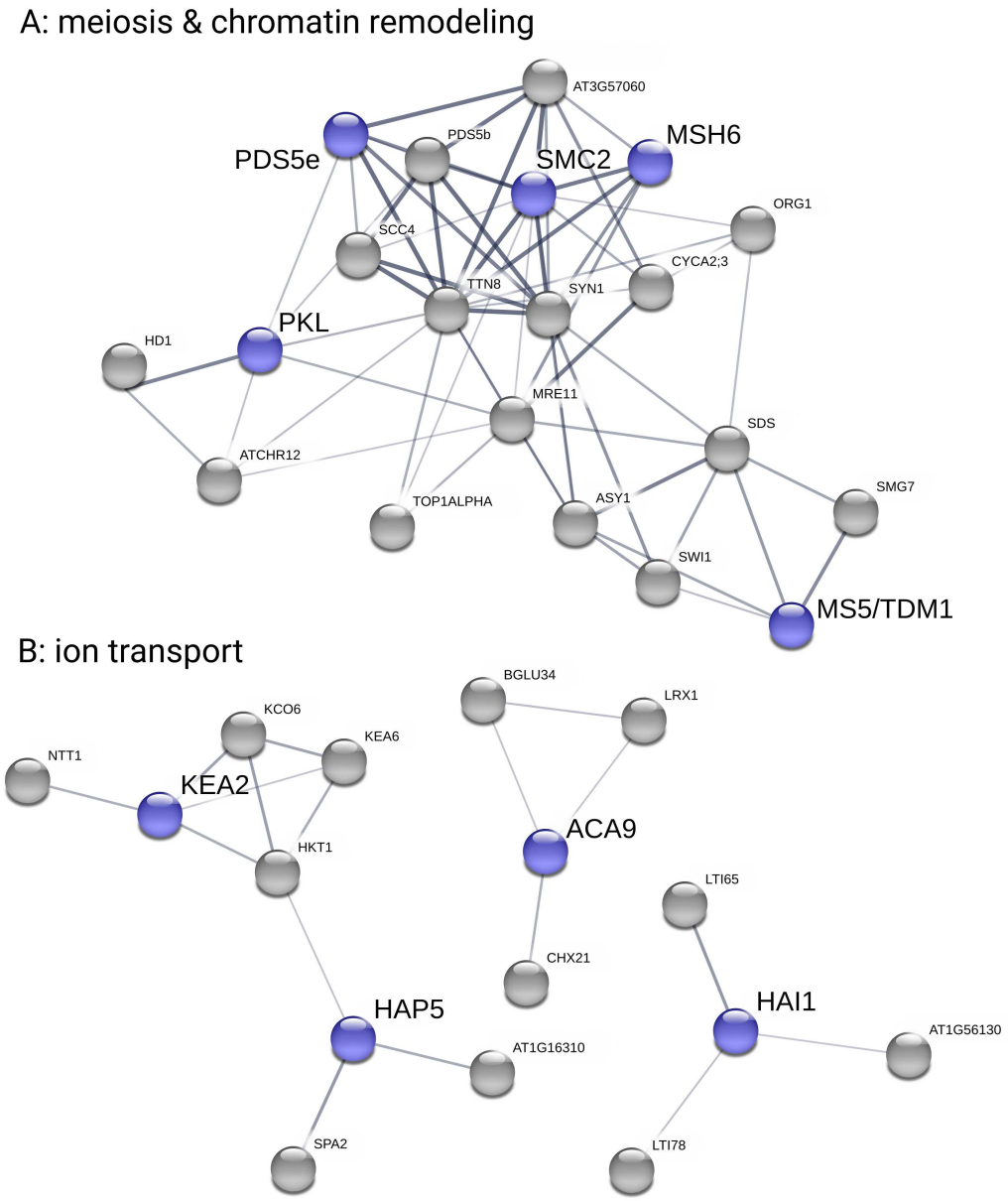

Figure 4. Evidence for functional parallelism between *C. amara* and *A. arenosa* following independent WGDs. Plots show *C. amara* candidate genes in blue and STRING-associated *A. arenosa* candidate genes in grey. We used only medium confidence associations and higher (increasing thickness of lines connecting genes indicates greater confidence). **A**, meiosis- and chromatin remodelling-related genes. **B**, ion transport-related genes.

Several large STRING clusters were evident among WGD adaptation candidates in *C. amara* and *A. arenosa* (Fig. 4). The largest of these clusters centre on genome maintenance, specifically meiosis and chromatin remodelling (Fig 4A), and ion homeostasis (especially K+ and Ca2+), along with stress (ABA) signalling (Fig 4B), consistent with the results of GO analysis. Taken together, both STRING and GO

363 analyses support our hypothesis of functional convergence of these processes following WGD in *C.*
364 *amara* and *A. arenosa.*
365

366 ## Conclusion

367 Given the expected shared challenges attendant to WGD in *C. amara* and *A. arenosa,* we hypothesised
368 at least partially convergent evolutionary responses to WGD. While we found obvious convergent
369 recruitment at the level of functional processes, we did not detect excess convergence at the genic
370 level. This was consistent with the probable absence of shared standing variation between these
371 species (51), which are 17 million years diverged. Nevertheless, we note that if any shared variation has
372 persisted, it was not selected upon convergently in both young autotetraploids, thus strengthening the
373 conclusion that the genes selected in response to WGD are not highly constrained between these two
374 species. The most prominent difference we observed here is the lack of an obvious coordinated
375 evolutionary response in genes stabilizing early meiotic chromosome segregation in *C. amara*, relative
376 to the striking coevolution of physically and functionally interacting proteins governing crossover
377 formation in *A. arenosa*. This could be explained to some extent by the observation that in *C. amara*
378 both diploids and autotetraploids are not uniformly meiotically stable, and autotetraploids may
379 therefore enjoy a less strict reliance on the generation of a high percentage of euploid gametes. This
380 may allow the decoupling of crossover reduction from broader changes across meiosis and other
381 processes we observe. This is not to say that we see no signal of WGD adaptation in *C. amara*: factors
382 governing timing during later meiosis, especially the exit from meiotic divisions as evidenced by the
383 interacting trio of *SMG7, SDS* and *MS5*, along with other chromatin remodelling factors and DNA repair-
384 related proteins, such as *MSH6* and *DAYSLEEPER* give very strong signals. The convergent functions we
385 did detect (other meiosis processes, chromosome organisation/chromatin remodelling, ABA signalling
386 and ion transport) provide first insights into the salient challenges associated with WGD.
387

388 We conclude that evolutionary solutions to WGD-associated challenges vary from case to case,
389 suggesting minimal constraint. This may explain how many species manage to thrive following WGD
390 and, once established as polyploids, experience evolutionary success. In fact, we envision that the
391 meiotic instability experienced by some WGD lineages, such as *C. amara*, could serve as a diversity-

392 generating engine promoting large effect genomic structural variation, as has been observed in
393 aggressive polyploid gliomas (3).
394

395 Materials and Methods

396 Reference Genome Assembly and Alignment

397 We generated a *de novo* assembly using the 10x Genomics Chromium approach. In brief, a single diploid
398 individual from pop LUZ (*SI Appendix*, Table S11) was used to generate a single Chromium library,
399 sequenced using 250PE mode on an Illumina sequencer, and assembled with Supernova version 2.0.0.
400 This assembly had an overall scaffold N50 of 1.82mb. An assessment of genome completeness using
401 BUSCO (version 3.0.2) (52) for the 2,251 contigs >=10kb was estimated at 94.8% (1365/1440 BUSCO
402 groups; *SI Appendix*, Table S12).
403

404 **BioNano Plant Extraction protocol**

405 High molecular weight DNA extraction and 10x synthetic long read library construction detailed
406 methods are provided in *SI Appendix*, Methods. The libraries were run at 250 paired end format on an
407 Illumina HiSeq.
408

409 **Sequencing and assembly and assembly QC**

410 Raw reads were subsampled to 90 M reads and assembled with Supernova 2.0.0 (10x Genomics), giving
411 a raw coverage of 60.30x and an effective coverage of 47.43x. The estimated molecule length was 44.15
412 kb. The assembly size, counting only scaffolds longer than 10kb was 159.53 Mb and the Scaffold N50
413 was 1.82MB. The k-mer estimate for the genome size was 225.39 MB, hence we are missing 16.61%
414 from the assembly by retaining only contigs longer than 10Kb. We further scaffolded the assembly using
415 the published *Cardamine hirsuta* genome using *graphAlign* (53) and *Nucmer* (54).
416

417 **Gene Calling and Annotation**

418 The 'plants set' database 'embryophyta_odb9.tar.gz' was downloaded from http://busco.ezlab.org/ and
419 used to assess orthologue presence/absence in our *C. amara* genome annotation. Running BUSCO gave
420 Augustus (55) results via BUSCO HMMs to infer where genes lie in the assembly and returning their
421 protein sequences. A blast (v. 2.2.4) database was built for Brassicales (taxid: 3699) by downloading ~
422 1.26M protein sequences from https://www.ncbi.nlm.nih.gov/taxonomy/ and the Augustus-predicted
423 proteins were annotated via Interproscan (56) and blast2go (57).
424

425 **Orthogrouping and Reciprocal Best Blast Hits**

426 We performed an orthogroup analysis using Orthofinder version 2.3.3 (58). to infer orthologous groups
427 (OGs) from four species (*C. amara, A. lyrata, A. thaliana, C. pyrenaica*). A total of 21,618 OGs were
428 found. Best reciprocal blast hits (RBHs) for *C. amara* and *A. thaliana* genes were found using BLAST
429 version 2.9.0. *C. amara* genes were then assigned an *A. thaliana* gene ID for GO enrichment analysis via
430 the following protocol: First, if the genes' OG contained only one *A. thaliana* gene ID, that gene ID was
431 used. If the OG contained more than one *A. thaliana* gene, then the RBH was taken. If there was no
432 RBH the *A. thaliana* gene ID, then the OG gene with the lowest E-value in a BLAST versus the TAIR10
433 database was taken. If no OG contained the *C. amara* gene, then the RBH was taken. Finally, if there
434 was no OG or RBH then the gene with the lowest E-value in a BLAST versus the TAIR10 database was
435 taken. BLASTs versus the TAIR10 database were performed during December 2019.

436
437 ## Population resequencing and genome scans for selection
438 **Sampling design**
439 To isolate genomic regions subjected to directional selection acting specifically between diploids and
440 autotetraploids, we sampled a set of two diploid and two tetraploid populations (Fig. 1C). We used
441 comparisons between populations of the same ploidy to constitute a null model for shared
442 heterogeneity in genetic differentiation arising through processes unrelated to WGD (following an
443 approach successfully applied in (21)).
444
445 **Library preparation and sequencing**
446 We extracted DNA in triplicate from 25 individuals for each of the following populations: CEZ (4x), PIC
447 (4x), VKR (2x), and LUZ (2x). All plants used for DNA extraction were verified for expected ploidy by flow
448 cytometry. We then pooled samples of each population, constructed Illumina Truseq libraries
449 (Illumina), and sequenced them on an Illumina NextSeq at a 150 base pair, paired-end specification.
450
451 **Data preparation, alignment, and genotyping**
452 Fastq files from the two runs were combined and concatenated to give an average of 30.5 million reads
453 per sample. Data processing steps are given in *SI Appendix*, Methods, along with variant calling steps.
454
455 **Population genetic structure**
456 We first calculated genome-wide between-population metrics (Nei's Fst (59) and allele frequency
457 difference). We calculated allele frequencies (AF) as the average AF of all the pools. The AF in individual
458 pools has been calculated as the fraction of the total number of reads supporting the alternative allele
459 (60). We used the python3 PoolSeqBPM pipeline, designed to input pooled data
460 (https://github.com/mbohutinska/PoolSeqBPM). Then we inferred relationships between populations
461 as genetic distances calculated over putatively neutral four-fold degenerate sites using principal
462 component analysis (PCA) implemented in *adegenet* (61).
463
464 **Window-based selection scan using a quartet design**
465 We performed a window-based Fst (59) scan for directional selection in *C. amara*, taking advantage of
466 quartet of two diploid and two autotetraploid populations (Fig. 1C). Using such quartet design, we
467 identified top candidate windows for selective sweeps associated with ploidy differentiation, while
468 excluding differentiation patterns private to a single population or ploidy-uninformative selective
469 sweeps. To do so, we calculated Fst for 1 kb windows with minimum 20 SNPs for all six population pairs
470 in the quartet (Fig. 1C) and ranked windows based on their Fst value. We excluded windows which were
471 top 1% outliers in diploid-diploid (dd in Fig. 1C) or autotetraploid-autotetraploid (tt) populations
472 contrasts, as they represent variation inconsistent with diploid-autotetraploid divergence but rather
473 signal local differentiation within a cytotype. Next, we assigned ranks to each window based on the Fst
474 values in four diploid-autotetraploid contrasts and identified windows being top 1% outliers of
475 minimum rank sum.
476
477 To account for possible confounding effect of comparing windows from genic and non-genic regions,
478 we calculated the number of base pairs overlapping with any gene within each window. There was not
479 any relationship between the proportion of genic space within a window and Fst (Pearson's $R^2 = -0.057$,
480 Figure S3), indicating that our analyses were unaffected by unequal proportion of genic space in a
481 window.

482 In *A. arenosa*, we performed window-based Fst scan for directional selection using the same criteria as
483 for *C. amara* (1kb windows, min 20 SNPs per window). We did not use the quartet design as the range-
484 wide dataset of 80 diploid and 40 autotetraploid individuals drawn from many populations assured
485 power to detect genomic regions with WGD-associated differentiation.
486
487 **FineMAV**
488 We adopted the Fine-Mapping of Adaptive Variation (fineMAV(22)), and modified it to fit the resources
489 available for *r*eference genome of *C. hirsuta*. Specifically, we replaced CADD, the functional score
490 available for amino acids in human reference (22, 62), by the Grantham score (63), which is a purely
491 theoretical amino acid substitution value, encoded in the Grantham matrix, where each element shows
492 the differences of physicochemical properties between two amino acids. Details on FineMAV data
493 processing are given in *SI Appendix*, Methods.
494
495 **Arabidopsis arenosa population genomic dataset**
496 We complemented our analysis of adaptation to WGD in *C. amara* with analysis of *A. arenosa,* based
497 on an expanded sampling (8) relative to the original *A. arenosa* WGD adaptation studies (13, 14). We
498 first aligned the short read sequences to the *A. lyrata* reference genome, called variants and filtered as
499 previously using the Genome Analysis Toolkit (GATK 3.5 and 3.6 (64)). We used a subset of the dataset
500 consisting of 80 diploid individuals (samples selected based on the highest mean depth of coverage)
501 and 40 tetraploid individuals from populations unaffected by secondary introgression from diploid
502 lineages (8). Such sub-sampling gave us a balanced number of 160 high-quality haploid genomes of
503 each ploidy suitable for selection scans. Finally, we filtered each subsampled dataset for genotype read
504 depth > 8 and maximum fraction of missing genotypes < 0.5 in each lineage. We calculated Fst using
505 python3 ScanTools pipeline (github.com/mbohutinska/ScanTools_ProtEvol). All subsequent analyses
506 were performed following the same procedure as with *C. amara* data.
507
508 **GO enrichment analysis**
509 To infer functions significantly associated with directional selection following WGD, we performed gene
510 ontology enrichment of gene list using the R package topGO (65), using *A. thaliana* orthologs of *C.*
511 *amara/A. lyrata* genes, obtained using biomaRt (66). We used Fisher's exact test with conservative
512 'elim' method, which tests for enrichment of terms from the bottom of the GO hierarchy to the top and
513 discards any genes that are significantly enriched in a descendant GO terms (67). We used 'biological
514 process' ontology with minimum node size 150 genes.
515
516 **Protein associations from STRING database**
517 We searched for association among *C. amara* and *A. arenosa* candidate genes using STRING (50)
518 database. We used multiple proteins search in *A. thaliana*, with text mining, experiments, databases,
519 co-expression, neighbourhood, gene fusion and co-occurrence as information sources. We used
520 minimum confidence 0.4 and retained only 1st shell associations (proteins that are directly associated
521 with the candidate protein: i.e., neighbouring circles in the network).
522
523 **Quantifying convergence**
524 We considered convergent candidates all candidate genes or significantly enriched GO categories that
525 overlapped across both species. Convergent candidate genes had to be members of the same
526 orthogroups (58). To test for higher than random number of overlapping items we used Fisher's Exact
527 Test for Count Data in R (68).

528
529 ## Cytological assessment of meiotic stability
530 **Chromosome preparation**
531 Whole young inflorescences were fixed in freshly prepared ethanol:acetic acid (3:1) overnight,
532 transferred into 70 % ethanol and later stored at -20 °C until use. Meiotic chromosome spreads were
533 prepared from anthers according to (69). Briefly, after washing in citrate buffer (10 mM sodium citrate,
534 pH 4.8), selected flower buds were digested using a 0.3 % mix of pectolytic enzymes (cellulase,
535 cytohelisase, pectolyase; Sigma-Aldrich Corp., St. Louis, MO) in citrate buffer for c. 3 h. Individual
536 anthers were dissected and spread in 20 µl of 60 % acetic acid on a microscope slide placed on a metal
537 hot plate (50 °C), fixed by ethanol:acetic acid (3:1) and the preparation was dried using a hair dryer.
538 SuiSI Table Slides were postfixed in freshly prepared 4 % formaldehyde in distilled water for 10 min and
539 air-dried. The preparations were stained with 4',6-diamidino-2-phenylindole (DAPI; 2 µg/ml) in
540 Vectashield (Vector Laboratories, Peterborough, UK). Fluorescence signals were analysed using an
541 Axioimager Z2 epifluorescence microscope (Zeiss, Oberkochen, Germany) and CoolCube CCD camera
542 (MetaSystems, Newton, MA).
543
544 **Meiotic stability scoring**
545 In diploids, chromosome spreads with 8 bivalents were scored as "stable meiosis", 7-6 as "partly
546 stable", 5-4 as "partly unstable", and <4 as "unstable". In autotetraploids, chromosome spreads with
547 16 bivalents were scored as "stable meiosis", 14-12 as "partly stable", 10-8 as "partly unstable", and <8
548 as "unstable". We report a mean value of meiotic stability for each ploidy calculated over "stable
549 meiosis" and over sum of "stable meiosis" and "partly stable" categories. Difference in meiotic stability
550 between diploids and autotetraploids (Fig. 3B) is reported for the sum of "stable" and "partly stable"
551 categories. However, considering only "stable meiosis" category does not qualitatively affect the results
552 (i.e. the degree of meiotic stability is significantly lower in tetraploids, $D = 125.7$, $df = 1$, $p < 0.0001$, GLM
553 with binomial errors). Photos of all spreads scored are shown in Figure S4.
554
555 ## Acknowledgements
556 The authors thank Veronika Konečná for assistance with the map figure and Doubravka Požárová and
557 Paolo Bartolić for help with field collections. This work was supported by the European Research Council
558 (ERC) under the European Union's Horizon 2020 research and innovation programme [grant number
559 ERC-StG 679056 HOTSPOT], via a grant to LY. Additional support was provided by Czech Science
560 Foundation (project 20-22783S to FK, 19-03442S to TM and 19-06632S), by Charles University (project
561 Primus/SCI/35 to FK), by the long-term research development project No. RVO 67985939 of the Czech
562 Academy of Sciences and by the CEITEC 2020 project (grant LQ1601).
563
564 ## Data Availability
565 Sequence data that support the findings of this study have been deposited in the Sequence Read
566 Archive (SRA; https://www.ncbi.nlm.nih.gov/sra) with the study codes SRP156117
567 702 (*A. arenosa* data, released) and SRPXXXXXX (*C. amara* data, released upon publication). All script
568 are available at github.com/mbohutinska/PoolSeqBPM (Fst-based selection scans and all following
569 analyses) and github.com/paajanen/meiosis_protein_evolution (fineMAV scan).
570
571 ## Author Contributions

LY conceived the study. MB, MA, PP, SB, TM and PM performed analyses. PM and TM performed laboratory experiments. PM, FK, SB, and MB performed field collections. LY and MB wrote the manuscript with input from all authors. All authors approved of the final manuscript.

Competing Interests statement

The authors declare no competing interests.

Materials & Correspondence

All requests should be addressed to Levi Yant at levi.yant@nottingham.ac.uk

581 # References

582 1. Y. Van De Peer, E. Mizrachi, K. Marchal, The evolutionary significance of polyploidy. *Nat. Rev. Genet.* **18**,
583 411–424 (2017).
584 2. K. Bomblies, A. Madlung, Polyploidy in the Arabidopsis genus. *Chromosom. Res.* **22**, 117–134 (2014).
585 3. L. Yant, K. Bomblies, Genome management and mismanagement—cell-level opportunities and
586 challenges of whole-genome duplication. *Genes Dev.* **29**, 2405–2419 (2015).
587 4. A. Lloyd, K. Bomblies, Meiosis in autopolyploid and allopolyploid Arabidopsis. *Curr. Opin. Plant Biol.* **30**,
588 116–122 (2016).
589 5. D. Y. Chao, *et al.*, Polyploids exhibit higher potassium uptake and salinity tolerance in Arabidopsis.
590 *Science (80-.).* **341**, 658–659 (2013).
591 6. J. J. Doyle, J. E. Coate, Polyploidy, the nucleotype, and novelty: The impact of genome doubling on the
592 biology of the cell. *Int. J. Plant Sci.* **180**, 1–52 (2019).
593 7. A. M. Selmecki, *et al.*, Polyploidy can drive rapid adaptation in yeast. *Nature* **519**, 349–351 (2015).
594 8. P. Monnahan, *et al.*, Pervasive population genomic consequences of genome duplication in Arabidopsis
595 arenosa. *Nat. Ecol. Evol.* **3**, 457–468 (2019).
596 9. S. Marburger, *et al.*, Interspecific introgression mediates adaptation to whole genome duplication. *Nat.*
597 *Commun.* (2019) https:/doi.org/10.1038/s41467-019-13159-5.
598 10. P. Baduel, S. Bray, M. Vallejo-Marin, F. Kolář, L. Yant, The "Polyploid Hop": Shifting challenges and
599 opportunities over the evolutionary lifespan of genome duplications. *Front. Ecol. Evol.* **6** (2018).
600 11. K. Bomblies, J. D. Higgins, L. Yant, Meiosis evolves: Adaptation to external and internal environments.
601 *New Phytol.* **208**, 306–323 (2015).
602 12. F. Kolář, *et al.*, Northern glacial refugia and altitudinal niche divergence shape genome-wide
603 differentiation in the emerging plant model Arabidopsis arenosa. *Mol. Ecol.* (2016)
604 https:/doi.org/10.1111/mec.13721.
605 13. J. D. Hollister, *et al.*, Genetic Adaptation Associated with Genome-Doubling in Autotetraploid
606 Arabidopsis arenosa. *PLoS Genet.* **8** (2012).
607 14. L. Yant, *et al.*, Meiotic adaptation to genome duplication in Arabidopsis arenosa. *Curr. Biol.* **23**, 2151–
608 2156 (2013).
609 15. P. J. Seear, *et al.*, A novel allele of ASY3 is associated with greater meiotic stability in autotetraploid
610 Arabidopsis lyrata. *PLoS Genet.* **in press** (2020).
611 16. X. C. Huang, D. A. German, M. A. Koch, Temporal patterns of diversification in Brassicaceae demonstrate
612 decoupling of rate shifts and mesopolyploidization events. *Ann. Bot.* **125**, 29–47 (2020).
613 17. J. Lihová, J. F. Aguilar, K. Marhold, G. N. Feliner, Origin of the disjunct tetraploid Cardamine amporitana
614 (Brassicaceae) assessed with nuclear and chloroplast DNA sequence data. *Am. J. Bot.* **91**, 1231–1242
615 (2004).
616 18. J. Zozomová-Lihová, *et al.*, Cytotype distribution patterns, ecological differentiation, and genetic
617 structure in a diploid– tetraploid contact zone of Cardamine amara. *Am. J. Bot.* **102**, 1380–1395 (2015).
618 19. K. Marhold, M. Huthmann, H. Hurka, Evolutionary history of the polyploid complex of Cardamine amara
619 (Brassicaceae): isozyme evidence. *Plant Syst. Evol.* **233**, 15–28 (2002).
620 20. K. Marhold, Taxonomic evaluation of the tetraploid populations of Cardamine amara (Brassicaceae)
621 from the Eastern Alps and adjacent areas. *Bot. Helv.* **109**, 67–84 (1999).
622 21. N. Vijay, *et al.*, Evolution of heterogeneous genome differentiation across multiple contact zones in a
623 crow species complex. *Nat. Commun.* **7** (2016).
624 22. M. Szpak, *et al.*, FineMAV: Prioritizing candidate genetic variants driving local adaptations in human
625 populations. *Genome Biol.* **19** (2018).
626 23. K. M. Culligan, J. B. Hays, Arabidopsis MutS homologs - AtMSH2, AtMSH3, AtMSH6, and a novel AtMSH7
627 - Form three distinct protein heterodimers with different specificities for mismatched DNA. *Plant Cell*
628 **12**, 991–1002 (2000).
629 24. S. Y. Wu, K. Culligan, M. Lamers, J. Hays, Dissimilar mispair-recognition spectra of Arabidopsis DNA-

630 mismatch-repair proteins MSH2·MSH6 (MutSα) and MSH2·MSH7 (MutSγ). *Nucleic Acids Res.* **31**, 6027–
631 6034 (2003).
632 25. X. Lu, *et al.*, The Arabidopsis MutS homolog AtMSH5 is required for normal meiosis. *Cell Res.* **18**, 589–
633 599 (2008).
634 26. S. Panizza, T. Tanaka, A. Hochwagen, F. Eisenhaber, K. Nasmyth, Pds5 cooperates with cohesion in
635 maintaining sister chromatid cohesion. *Curr. Biol.* **10**, 1557–1564 (2000).
636 27. N. U. Siddiqui, P. E. Stronghill, R. E. Dengler, C. A. Hasenkampf, C. D. Riggs, Mutations in Arabidopsis
637 condensin genes disrupt embryogenesis, meristem organization and segregation of homologous
638 chromosomes during meiosis. *Development* **130**, 3283–3295 (2003).
639 28. C. M. Liu, D. W. Meinke, The titan mutants of Arabidopsis are disrupted in mitosis and cell cycle control
640 during seed development. *Plant J.* **16**, 21–31 (1998).
641 29. H. Shaked, N. Avivi-Ragolsky, A. A. Levy, Involvement of the arabidopsis SWI2/SNF2 chromatin
642 remodeling gene family in DNA damage response and recombination. *Genetics* **173**, 985–994 (2006).
643 30. J. Ogas, S. Kaufmann, J. Henderson, C. Somerville, PICKLE is a CHD3 chromatin-remodeling factor that
644 regulates the transition from embryonic to vegetative development in Arabidopsis. *Proc. Natl. Acad. Sci.*
645 *U. S. A.* **96**, 13839–13844 (1999).
646 31. E. Perruc, N. Kinoshita, L. Lopez-Molina, The role of chromatin-remodeling factor PKL in balancing
647 osmotic stress responses during Arabidopsis seed germination. *Plant J.* **52**, 927–936 (2007).
648 32. X. Kang, *et al.*, HRB2 and BBX21 interaction modulates Arabidopsis ABI5 locus and stomatal aperture.
649 *Plant Cell Environ.* **41**, 1912–1925 (2018).
650 33. E. Aichinger, C. B. R. Villar, R. di Mambro, S. Sabatini, C. Köhler, The CHD3 chromatin remodeler PICKLE
651 and polycomb group proteins antagonistically regulate meristem activity in the Arabidopsis root. *Plant*
652 *Cell* **23**, 1047–1060 (2011).
653 34. Y. Jing, Q. Guo, R. Lin, The Chromatin-Remodeling Factor PICKLE Antagonizes Polycomb Repression of FT
654 to Promote Flowering. *Plant Physiol.* **181**, 656–668 (2019).
655 35. P. Bundock, P. Hooykaas, An Arabidopsis hAT-like transposase is essential for plant development.
656 *Nature* **436**, 282–284 (2005).
657 36. K. Tamura, Y. Adachi, K. Chiba, K. Oguchi, H. Takahashi, Identification of Ku70 and Ku80 homologues in
658 Arabidopsis thaliana: Evidence for a role in the repair of DNA double-strand breaks. *Plant J.* **29**, 771–781
659 (2002).
660 37. M. (Leiden U. Knip, "Daysleeper : from genomic parasite to indispensable gene." (2012).
661 38. J. Glover, M. Grelon, S. Craig, A. Chaudhury, E. Dennis, Cloning and characterization of MS5 from
662 Arabidopsis: A gene critical in male meiosis. *Plant J.* **15**, 345–356 (1998).
663 39. M. Cifuentes, *et al.*, TDM1 Regulation Determines the Number of Meiotic Divisions. *PLoS Genet.* **12**
664 (2016).
665 40. D. Kawa, *et al.*, SnRK2 Protein Kinases and mRNA Decapping Machinery Control Root Development and
666 Response to Salt. *Plant Physiol.* **182**, 361–377 (2020).
667 41. H. Fujii, P. E. Verslues, J. K. Zhu, Arabidopsis decuple mutant reveals the importance of SnRK2 kinases in
668 osmotic stress responses in vivo. *Proc. Natl. Acad. Sci. U. S. A.* **108**, 1717–1722 (2011).
669 42. S. R. Cutler, P. L. Rodriguez, R. R. Finkelstein, S. R. Abrams, Abscisic Acid: Emergence of a Core Signaling
670 Network. *Annu. Rev. Plant Biol.* **61**, 651–679 (2010).
671 43. M. E. Williams, *et al.*, Mutations in the Arabidopsis phosphoinositide phosphatase gene SAC9 lead to
672 overaccumulation of PtdIns(4,5)P2 and constitutive expression of the stress-response pathway. *Plant*
673 *Physiol.* **138**, 686–700 (2005).
674 44. B. C. Meyers, M. Morgante, R. W. Michelmore, TIR-X and TIR-NBS proteins: Two new families related to
675 disease resistance TIR-NBS-LRR proteins encoded in Arabidopsis and other plant genomes. *Plant J.* **32**,
676 77–92 (2002).
677 45. A. V. Klepikova, A. S. Kasianov, E. S. Gerasimov, M. D. Logacheva, A. A. Penin, A high resolution map of
678 the Arabidopsis thaliana developmental transcriptome based on RNA-seq profiling. *Plant J.* **88**, 1058–
679 1070 (2016).

680 46. H. H. Kunz, *et al.*, Plastidial transporters KEA1, -2, and -3 are essential for chloroplast osmoregulation,
681 integrity, and pH regulation in Arabidopsis. *Proc. Natl. Acad. Sci. U. S. A.* **111**, 7480–7485 (2014).
682 47. A. B. Stephan, H. H. Kunz, E. Yang, J. I. Schroeder, Rapid hyperosmotic-induced Ca2+ responses in
683 Arabidopsis thaliana exhibit sensory potentiation and involvement of plastidial KEA transporters. *Proc.*
684 *Natl. Acad. Sci. U. S. A.* **113**, E5242–E5249 (2016).
685 48. J. M. Colmenero-Flores, *et al.*, Identification and functional characterization of cation-chloride
686 cotransporters in plants. *Plant J.* **50**, 278–292 (2007).
687 49. Hejný Slavomil, Slavík Bohumil, *Květena České republiky 3* (Academia, 2003).
688 50. D. Szklarczyk, *et al.*, STRING v10: Protein-protein interaction networks, integrated over the tree of life.
689 *Nucleic Acids Res.* **43**, D447–D452 (2015).
690 51. R. R. Hudson, J. A. Coyne, Mathematical consequences of the genealogical species concept. *Evolution*
691 *(N. Y).* **56**, 1557–1565 (2002).
692 52. M. Seppey, M. Manni, E. M. Zdobnov, "BUSCO: Assessing genome assembly and annotation
693 completeness" in *Methods in Molecular Biology*, (2019), pp. 227–245.
694 53. J. B. Spalding, P. J. Lammers, BLAST Filter and GraphicAlign: Rule-based formation and analysis of sets of
695 related DNA and protein sequences. *Nucleic Acids Res.* **32** (2004).
696 54. G. Marçais, *et al.*, MUMmer4: A fast and versatile genome alignment system. *PLoS Comput. Biol.* **14**
697 (2018).
698 55. M. Stanke, S. Waack, Gene prediction with a hidden Markov model and a new intron submodel in
699 *Bioinformatics*, (2003).
700 56. E. Quevillon, *et al.*, InterProScan: Protein domains identifier. *Nucleic Acids Res.* **33** (2005).
701 57. A. Conesa, S. Götz, Blast2GO: A comprehensive suite for functional analysis in plant genomics. *Int. J.*
702 *Plant Genomics* **2008** (2008).
703 58. E. D.M., K. S., OrthoFinder2: fast and accurate phylogenomic orthology analysis from gene sequences.
704 *bioRxiv*, 466201 (2018).
705 59. M. Nei, Genetic Distance between Populations. *Am. Nat.* (1972) https:/doi.org/10.1086/282771.
706 60. S. Anand, *et al.*, Next generation sequencing of pooled samples: Guideline for variants' filtering. *Sci. Rep.*
707 **6** (2016).
708 61. T. Jombart, I. Ahmed, adegenet 1.3-1: New tools for the analysis of genome-wide SNP data.
709 *Bioinformatics* **27**, 3070–3071 (2011).
710 62. P. Rentzsch, D. Witten, G. M. Cooper, J. Shendure, M. Kircher, CADD: Predicting the deleteriousness of
711 variants throughout the human genome. *Nucleic Acids Res.* **47**, D886–D894 (2019).
712 63. R. Grantham, Amino acid difference formula to help explain protein evolution. *Science (80-.).* **185**, 862–
713 864 (1974).
714 64. A. McKenna, *et al.*, The genome analysis toolkit: A MapReduce framework for analyzing next-generation
715 DNA sequencing data. *Genome Res.* **20**, 1297–1303 (2010).
716 65. A. Alexa, J. Rahnenführer, Gene set enrichment analysis with topGO. *Bioconductor Improv.* (2007).
717 66. D. Smedley, *et al.*, BioMart - Biological queries made easy. *BMC Genomics* (2009)
718 https:/doi.org/10.1186/1471-2164-10-22.
719 67. S. Grossmann, S. Bauer, P. N. Robinson, M. Vingron, Improved detection of overrepresentation of Gene-
720 Ontology annotations with parent-child analysis. *Bioinformatics* **23**, 3024–3031 (2007).
721 68. R. R Development Core Team, *R: A Language and Environment for Statistical Computing* (2011).
722 69. T. Mandáková, K. Marhold, M. A. Lysak, The widespread crucifer species Cardamine flexuosa is an
723 allotetraploid with a conserved subgenomic structure. *New Phytol.* **201**, 982–992 (2014).
724

Supplemental Information for:

Genomic novelty and process-level convergence in adaptation to whole genome duplication

Magdalena Bohutínská[1,2], Mark Alston[3], Patrick Monnahan[3], Terezie Mandáková[4], Sian Bray[3], Pirita Paajanen[3], Filip Kolář[1,2,5], and Levi Yant[6]*

1. Department of Botany, Faculty of Science, Charles University, Prague, Czech Republic
2. Institute of Botany, The Czech Academy of Sciences, Průhonice, Czech Republic
3. Department of Cell and Developmental Biology, John Innes Centre, Norwich Research Park, Norwich, UK
4. CEITEC – Central European Institute of Technology, and Faculty of Science, Masaryk University, Kamenice, Czech Republic
5. Natural History Museum, University of Oslo, Oslo, Norway
6. Future Food Beacon and School of Life Sciences University of Nottingham, Nottingham, UK

Magdalena Bohutínská and Mark Alston contributed equally.

***Author for correspondence:** Levi Yant

Email: levi.yant@nottingham.ac.uk

This PDF file includes:

Supplemental Materials and Methods
Figs. S1 to S4

Other supplementary materials for this manuscript include the following:

Datasets S1 to S12

31 ## Supplemental Materials and Methods
32
33 **BioNano Plant Extraction protocol**
34 Fresh young leaves of the *C. amara* accession LUZ were collected after 48-hour treatment in the dark.
35 DNA was extracted by the Earlham Institute's Platforms and Pipelines group following an IrysPrep
36 "Fix'n'Blend" Plant DNA extraction protocol supplied by BioNano Genomics. 2.5 g of fresh young leaves
37 were fixed with 2% formaldehyde. After washing, leaves were disrupted and homogenized in the
38 presence of an isolation buffer containing PVP10 and BME to prevent oxidation of polyphenols. Triton
39 X-100 was added to facilitate the release of nuclei from the broken cells. The nuclei were then purified
40 on a Percoll cushion. A nuclei phase was taken and washed several times in isolation buffer before
41 embedding into low melting point agarose. Two plugs of 90 µl were cast using the CHEF Mammalian
42 Genomic DNA Plug Kit (Bio-Rad 170-3591). Once set at 4°C the plugs were added to a lysis solution
43 containing 200 µl proteinase K (QIAGEN 158920) and 2.5 ml of BioNano lysis buffer in a 50 ml conical
44 tube. These were put at 50°C for 2 hours on a thermomixer, making a fresh proteinase K solution to
45 incubate overnight. The 50 ml tubes were then removed from the thermomixer for 5 minutes before
46 50 µl RNAse A (Qiagen158924) was added and the tubes returned to the thermomixer for a further
47 hour at 37°C. The plugs were then washed 7 times in Wash Buffer supplied in Chef kit and 7 times in
48 1xTE. One plug was removed and melted for 2 minutes at 70°C followed by 5 minutes at 43°C before
49 adding 10 µl of 0.2 U /µl of GELase (Cambio Ltd G31200). After 45 minutes at 43°C the melted plug was
50 dialysed on a 0.1 µM membrane (Millipore VCWP04700) sitting on 15 ml of 1xTE in a small petri dish.
51 After 2 hours the sample was removed with a wide bore tip and mixed gently 5 times and left overnight
52 at 4°C.
53
54 **10X library construction**
55 DNA material was diluted to 0.5ng/ul with EB (Qiagen) and checked with a QuBit Flourometer 2.0
56 (Invitrogen) using the QuBit dsDNA HS Assay kit (Table S11). The Chromium User Guide was followed
57 as per the manufacturer's instructions (10X Genomics, CG00043, Rev A). The final library was quantified
58 using qPCR (KAPA Library Quant kit [Illumina] and ABI Prism qPCR Mix, Kapa Biosystems). Sizing of the
59 library fragments was checked using a Bioanalyzer (High Sensitivity DNA Reagents, Agilent). Samples
60 were pooled based on the molarities calculated using the two QC measurements. The library was
61 clustered at 8 pM with a 1% spike in of PhiX library (Illumina). The pool was run on a HiSeq2500 150bp
62 Rapid Run V2 mode (Illumina). The following run metrics were applied: Read 1: 250 cycles, Index 1: 8
63 cycles, Index 2: 0 cycles and Read 2: 250 cycles.
64
65 **Data preparation, alignment, and genotyping**
66 Fastq files from the two runs were combined and concatenated to give an average of 30.5 million reads
67 per sample. Adapter sequences were removed via the cutadapt software (version 1.9.1) (1) and quality
68 trimmed via Sickle (version 33) (2) to generate only high-quality reads (Phred score >=30) of 30bp or
69 more, resulting in an average of 27.9 million reads per sample. Using samtools (v. 1.7) (3) and bwa (v.
70 0.7.12) (4) software, the quality-filtered reads were aligned against two references: 89.3% of reads

mapped to our *C. amara* assembly, while only 74.5% to *C. hirsuta*. We retained only the alignment to *C. amara* for all analysis. Using the picard software tool (v. 1.134) (5), first duplicate reads were removed via 'MarkDuplicates' followed by the addition of read group IDs to the bam files via 'AddOrReplaceReadGroups'. Finally, to handle the presence of indels, GATK (v. 3.6.0) (6) was used to realign reads to the *C. amara* assembly via 'RealignerTargetCreator' and 'IndelRealigner'.

Variant Calling

Text files describing sample populations and ploidy were prepared, and variants called for the 12 bam files using Freebayes (v. 1.1.0.46)(7) to generate a single VCF output. Due to working with pooled (high ploidy) samples, Freebayes was run with '--pooled-discrete' (assumes samples result from pooled sequencing). In addition, the software was restricted to biallelic sites ('--use-best-n-alleles 2') and indel sites were excluded ('--no-indels'). The VCF was filtered via bcftools (v 1.8) (8) to remove sites where the read depth was < 10 or greater than 1.6x the second mode (determined as 1.6 x 31 = 50, Figure S2).

FineMAV

We downloaded coding sequences from the *C. hirsuta* genomic resources web site http://chi.mpipz.mpg.de/download/annotations/carhr38.cds.fa and mapped to *C. amara* using gmap. The resulting sam file was converted to bam-format, sorted and indexed via samtools (v. 1.7) (3), and then converted to GTF-format via the 'convert' script in Mikado (v1.2.3) (9) which was subsequently used to build a snpEFF (v. 4.3) (10) database. We estimated the population genetic component of fineMAV (see (11) for details on calculations) using allele frequency information at each site (considering minor frequency allele as derived) and DAP parameter of 3.5. Finally, for each amino acid substitution, we assigned Grantham scores, together with population genetic component of fineMAV, using a custom scripts in Python 2.7.10 and the Biopython 1.69 package. We identified the top 1% outliers and considered them the final candidates identified in fineMAV analysis. All the calculations were performed using code available at (github.com/paajanen/meiosis_protein_evolution).

Supplemental References

1. M. Martin, Cutadapt removes adapter sequences from high-throughput sequencing reads. *EMBnet.journal* **17**, 10 (2011).
2. N. Joshi, J. Fass, Sickle: A sliding-window, adaptive, quality-based trimming tool for FastQ files (Version 1.33) [Software]. *Available at https://github.com/najoshi/sickle.*, 2011 (2011).
3. H. Li, *et al.*, The Sequence Alignment/Map format and SAMtools. *Bioinformatics* **25**, 2078–2079 (2009).
4. H. Li, R. Durbin, Fast and accurate short read alignment with Burrows-Wheeler transform. *Bioinformatics* **25**, 1754–1760 (2009).
5. Broad Institute, Picard Tools - By Broad Institute. *Github* (2009).
6. A. McKenna, *et al.*, The genome analysis toolkit: A MapReduce framework for analyzing next-generation DNA sequencing data. *Genome Res.* **20**, 1297–1303 (2010).
7. E. Garrison, G. Marth, Haplotype-based variant detection from short-read sequencing (2012).
8. V. Narasimhan, *et al.*, BCFtools/RoH: A hidden Markov model approach for detecting autozygosity from next-generation sequencing data. *Bioinformatics* (2016) https:/doi.org/10.1093/bioinformatics/btw044.
9. L. Venturini, S. Caim, G. G. Kaithakottil, D. L. Mapleson, D. Swarbreck, Leveraging multiple transcriptome assembly methods for improved gene structure annotation. *Gigascience* **7** (2018).
10. P. Cingolani, *et al.*, A program for annotating and predicting the effects of single nucleotide polymorphisms, SnpEff: SNPs in the genome of Drosophila melanogaster strain w1118; iso-2; iso-3. *Fly (Austin).* **6**, 80–92 (2012).
11. M. Szpak, *et al.*, FineMAV: Prioritizing candidate genetic variants driving local adaptations in human populations. *Genome Biol.* **19** (2018).

Supplemental Figures

Figure S1

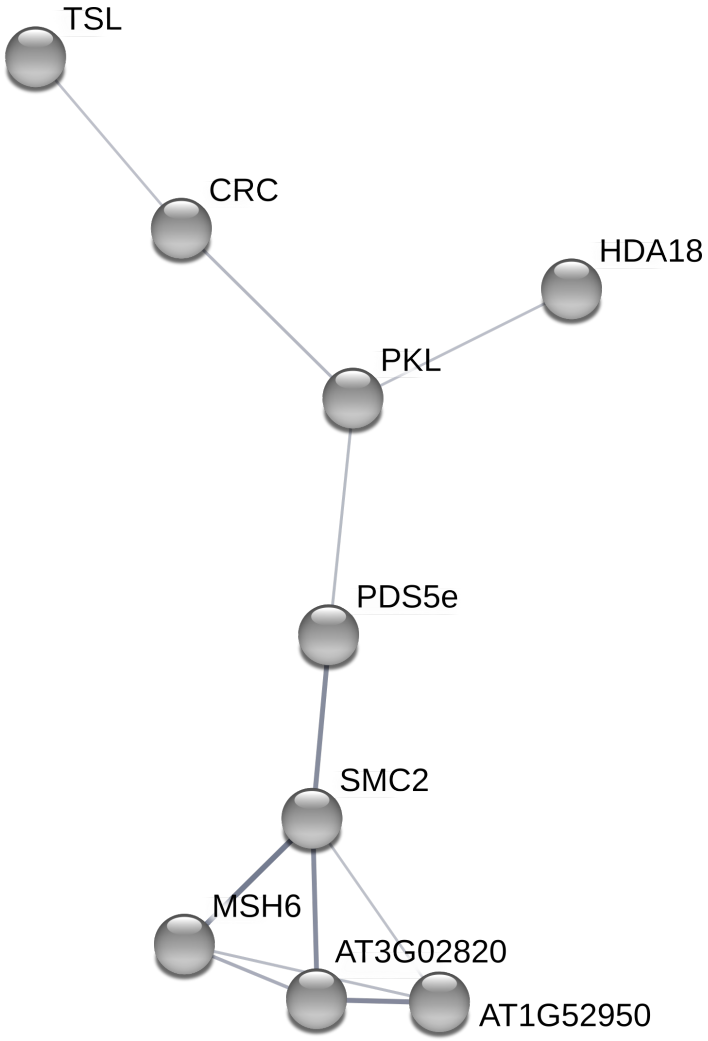

Figure S1: *C. amara* candidate meiosis gene associations as identified by STRING. We used only medium confidence associations and higher (shown as thickness of lines connecting genes).

Figure S2

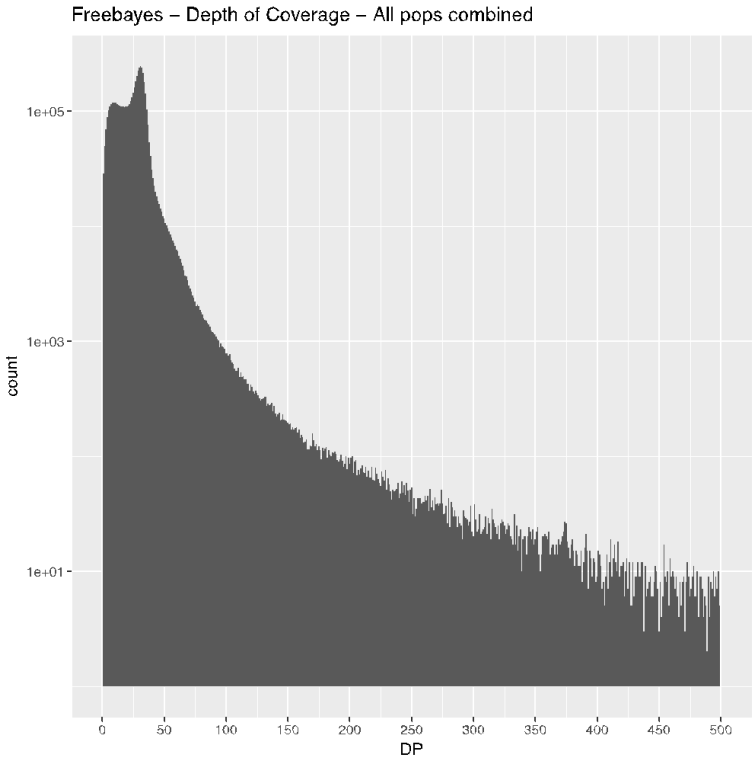

Figure S2: Distribution of read depth over all sequenced samples.

133 **Figure S3**

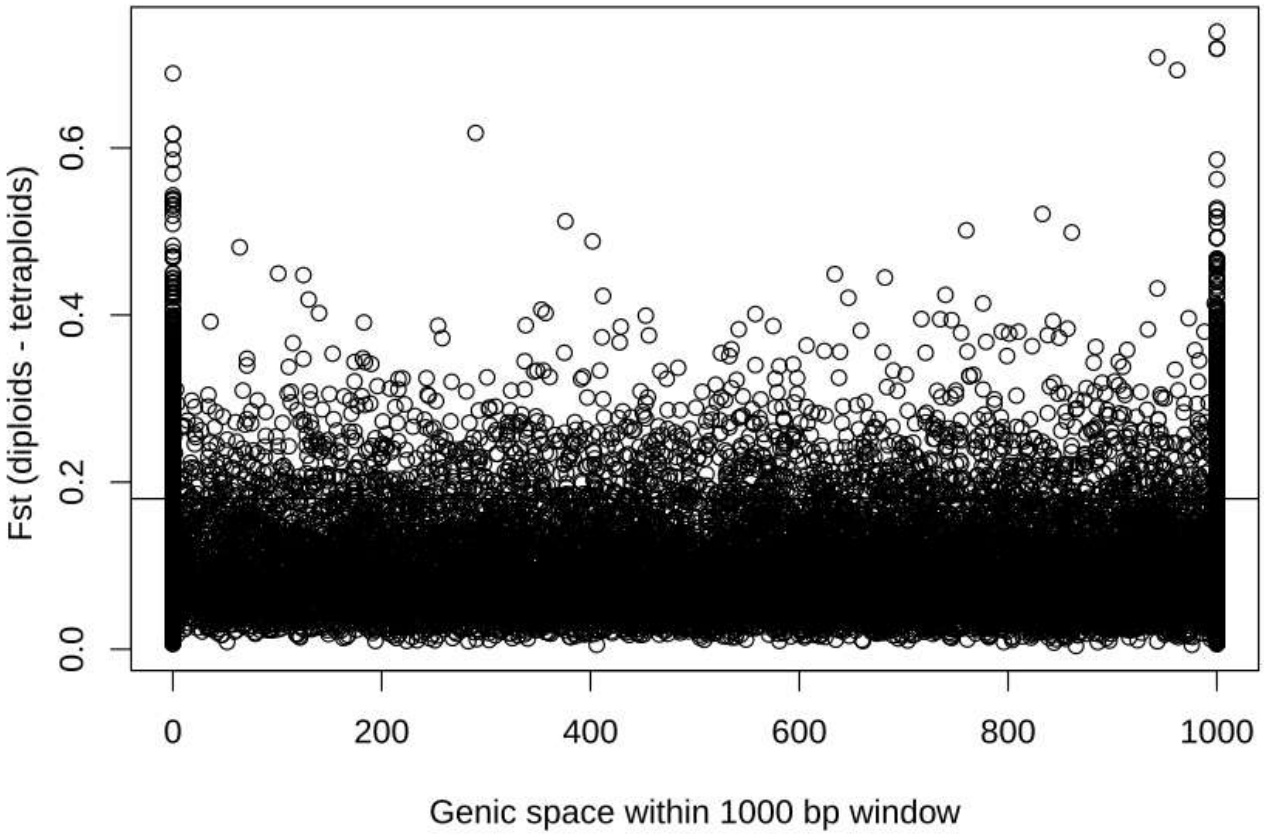

134

135 **Figure S3:** Relationship between the proportion of genic space within a window and Fst.

Figure S4. DAPI-stained meiotic (metaphase I) chromosomes of diploid (2n = 16; VKR6, VKR8, LUZ3, LUZ8, LUZ10, LUZ11, LUZ15) and tetraploid (2n = 32; CEZ7, PIC1, PIC5, PIC9, PIC11, PIC14, PIC1*8)* individuals of *Cardamine amara*. Scale bars = 10 µm.

VKR6

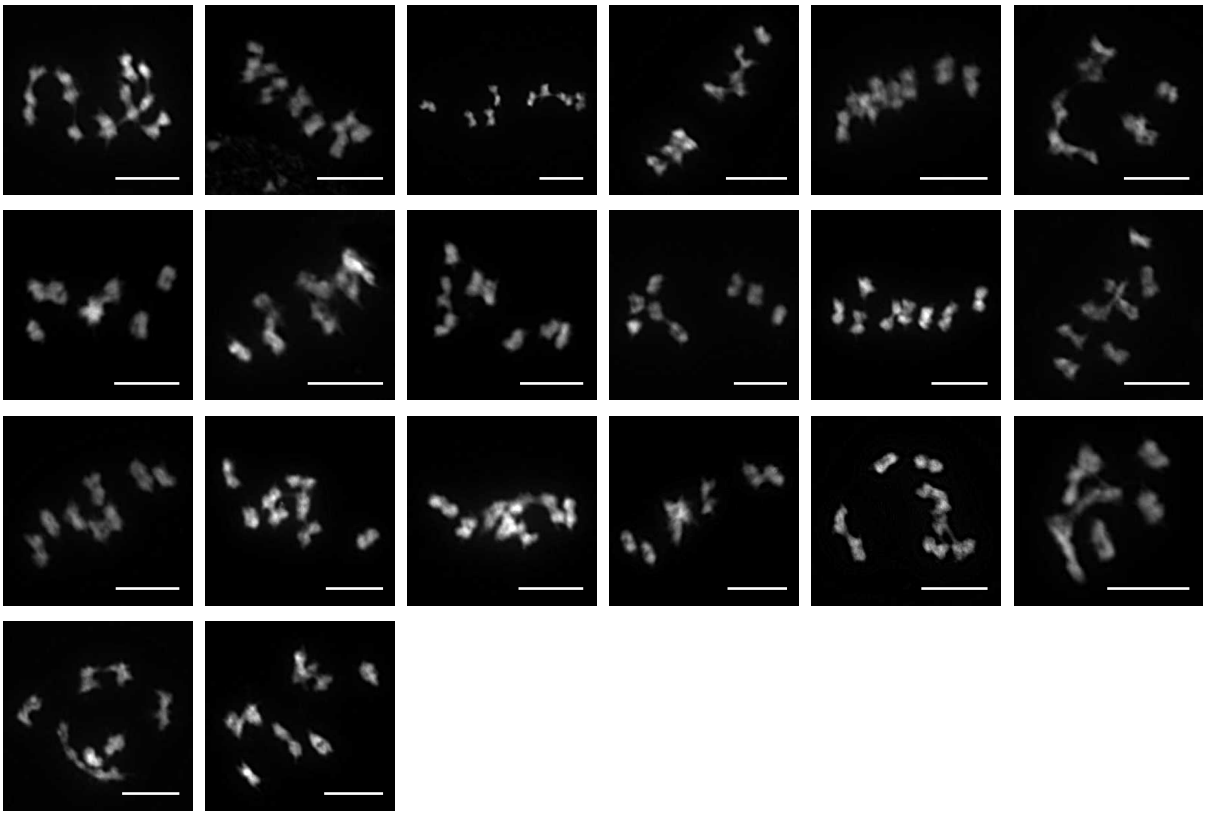

VKR8

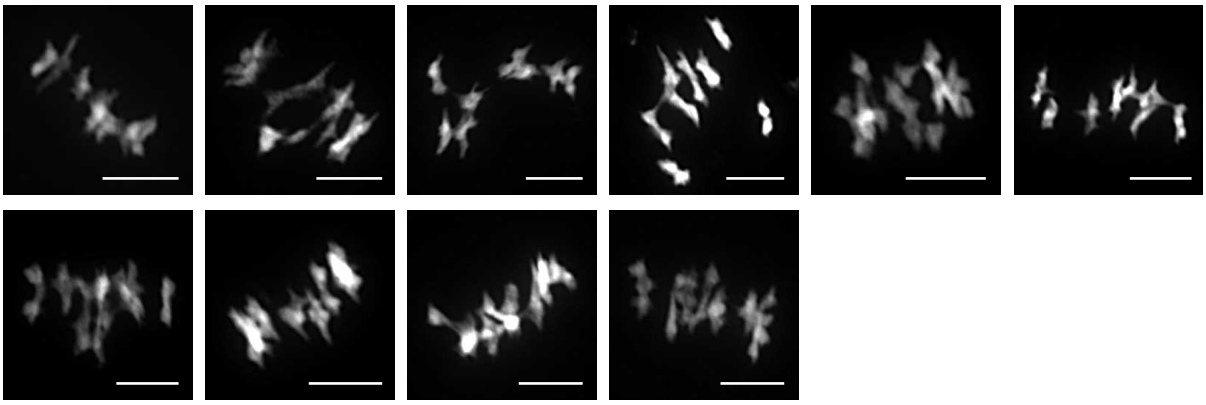

LUZ3

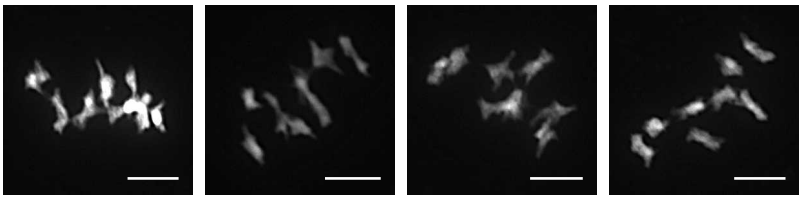

LUZ8

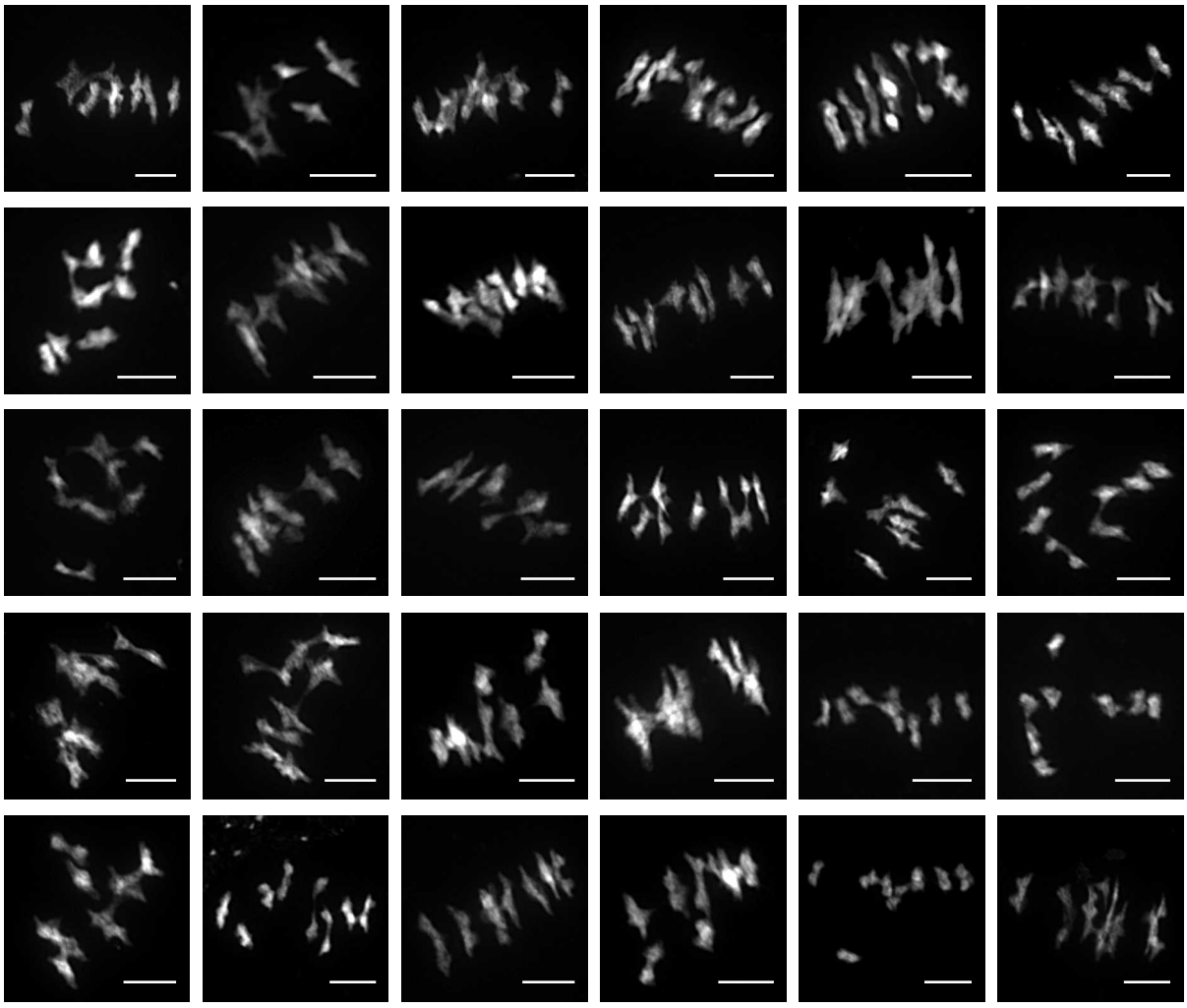

LUZ10

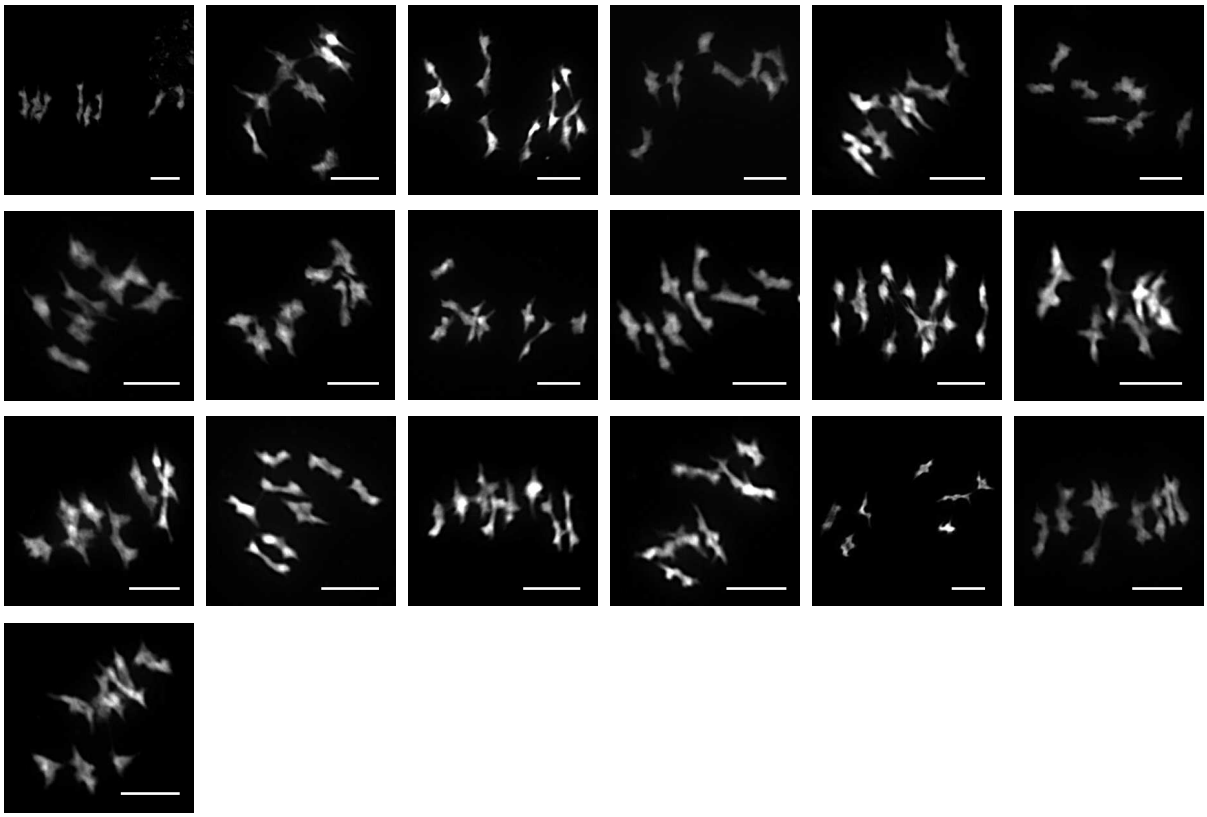

LUZ11

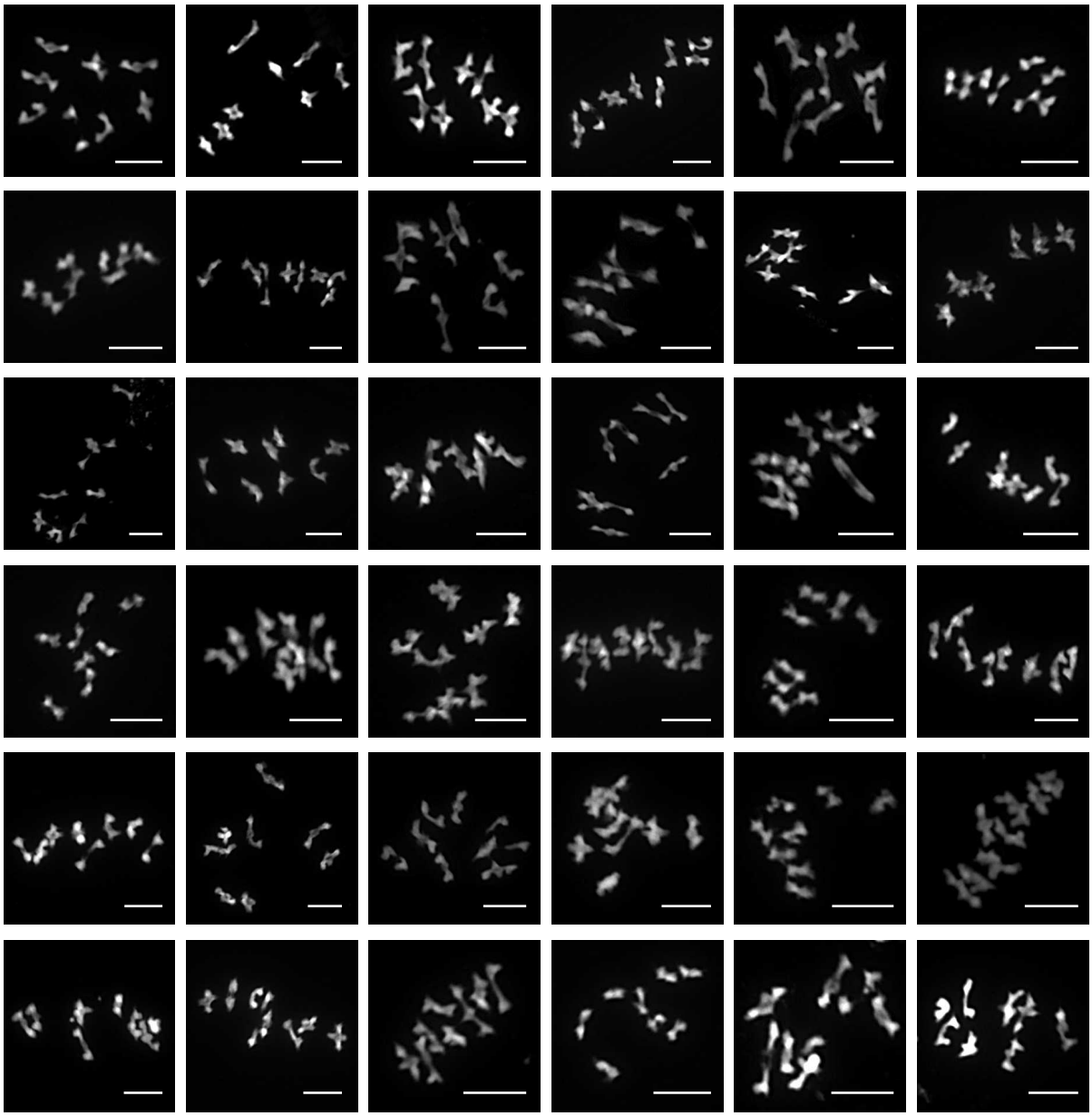

LUZ15

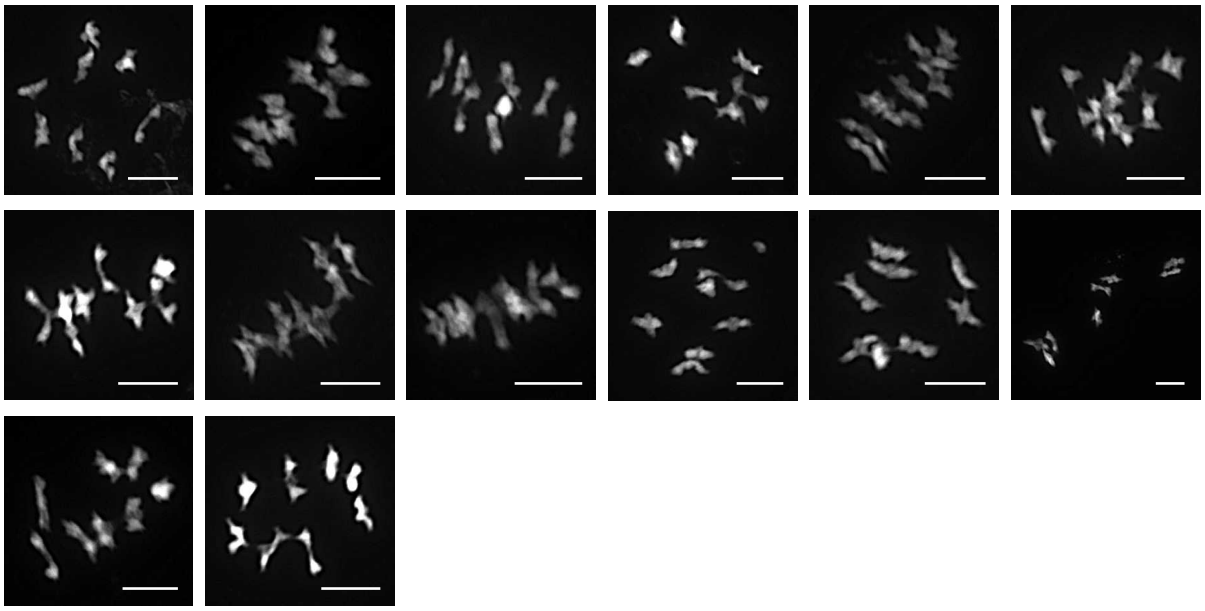

CEZ7

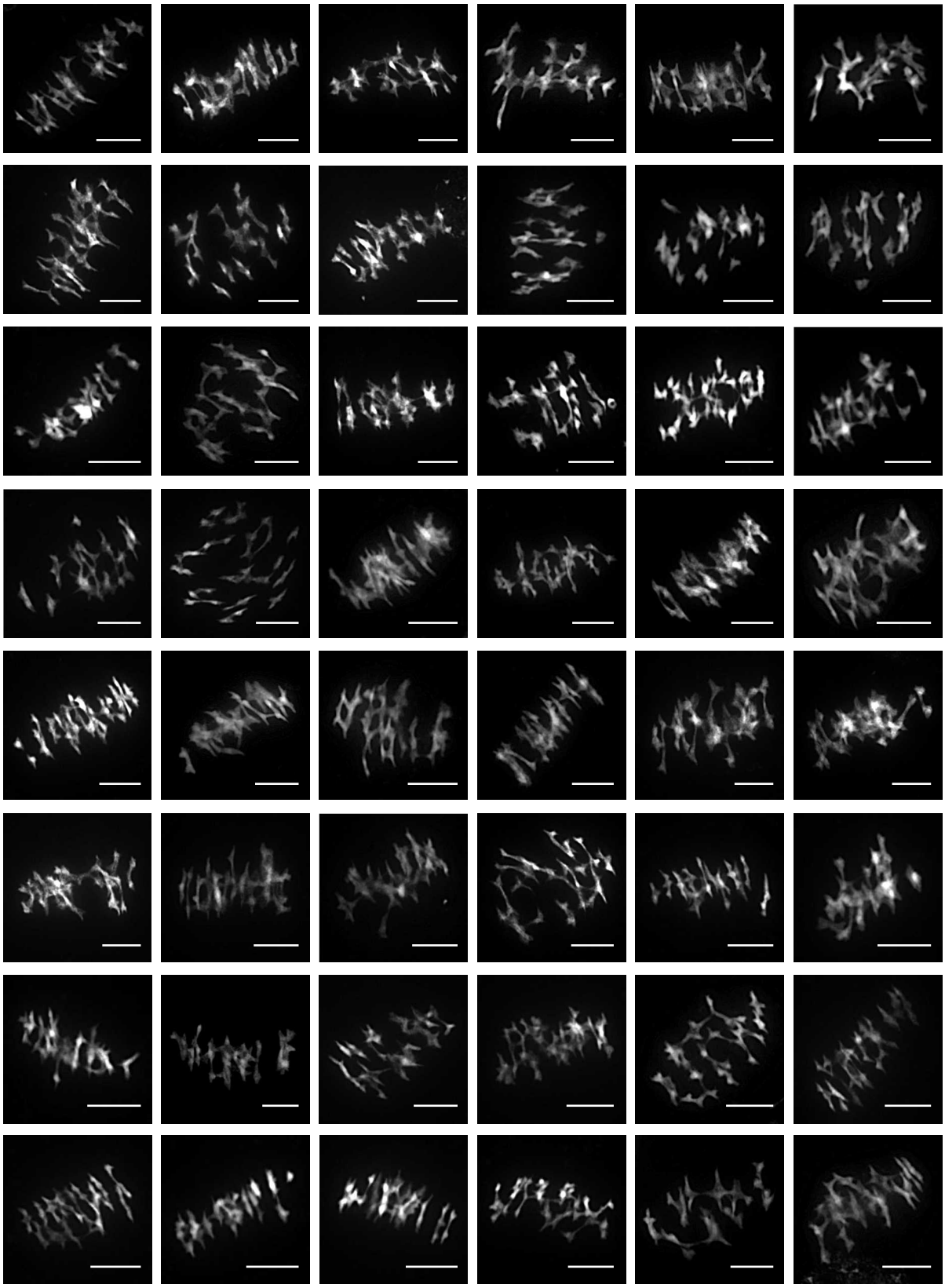

CEZ7 (cont.)

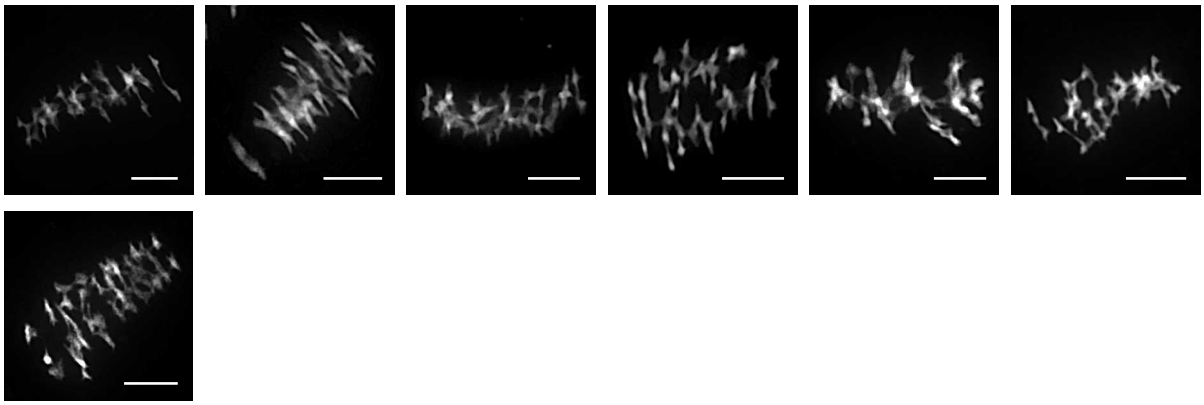

PIC1

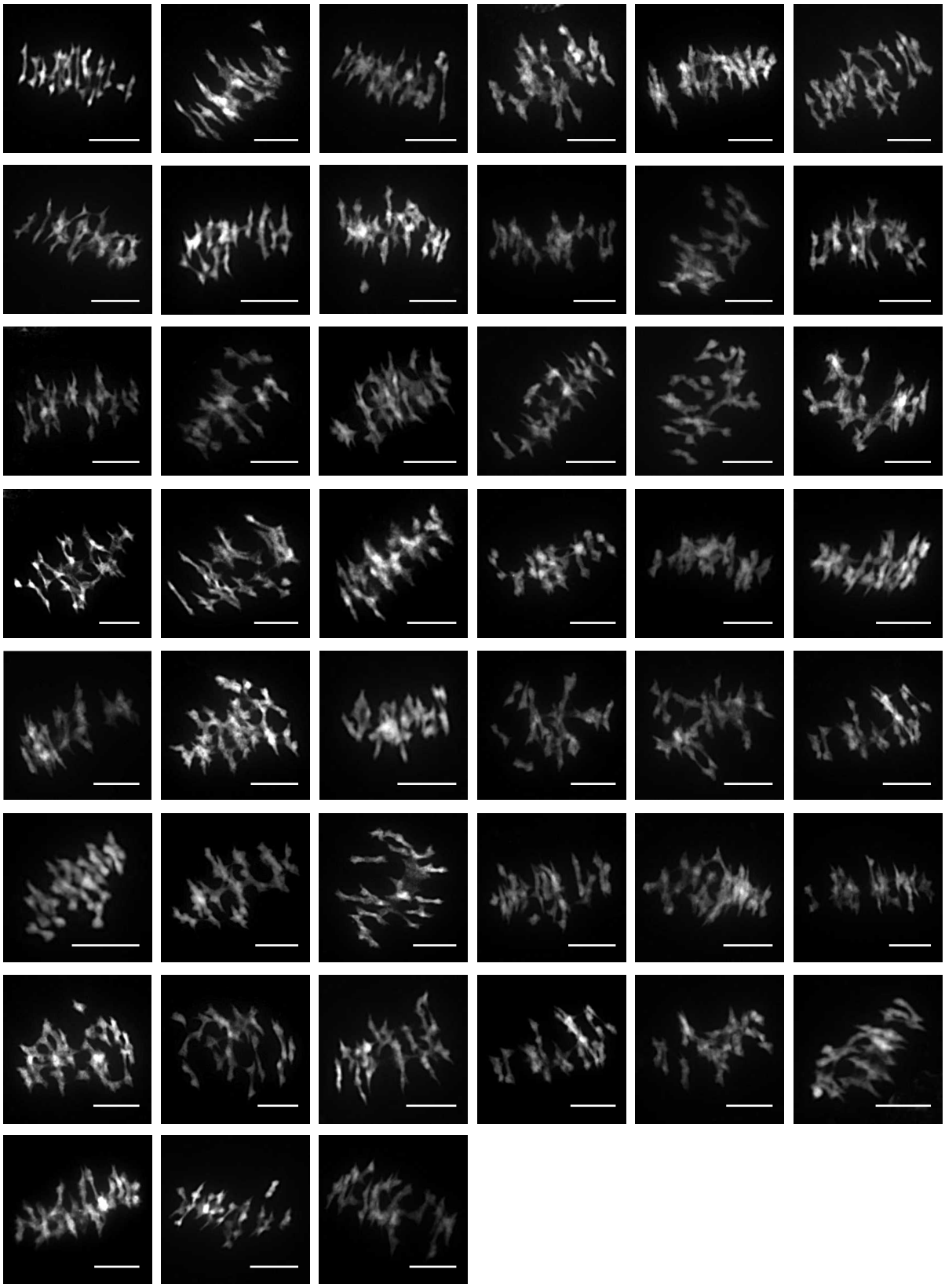

PIC5

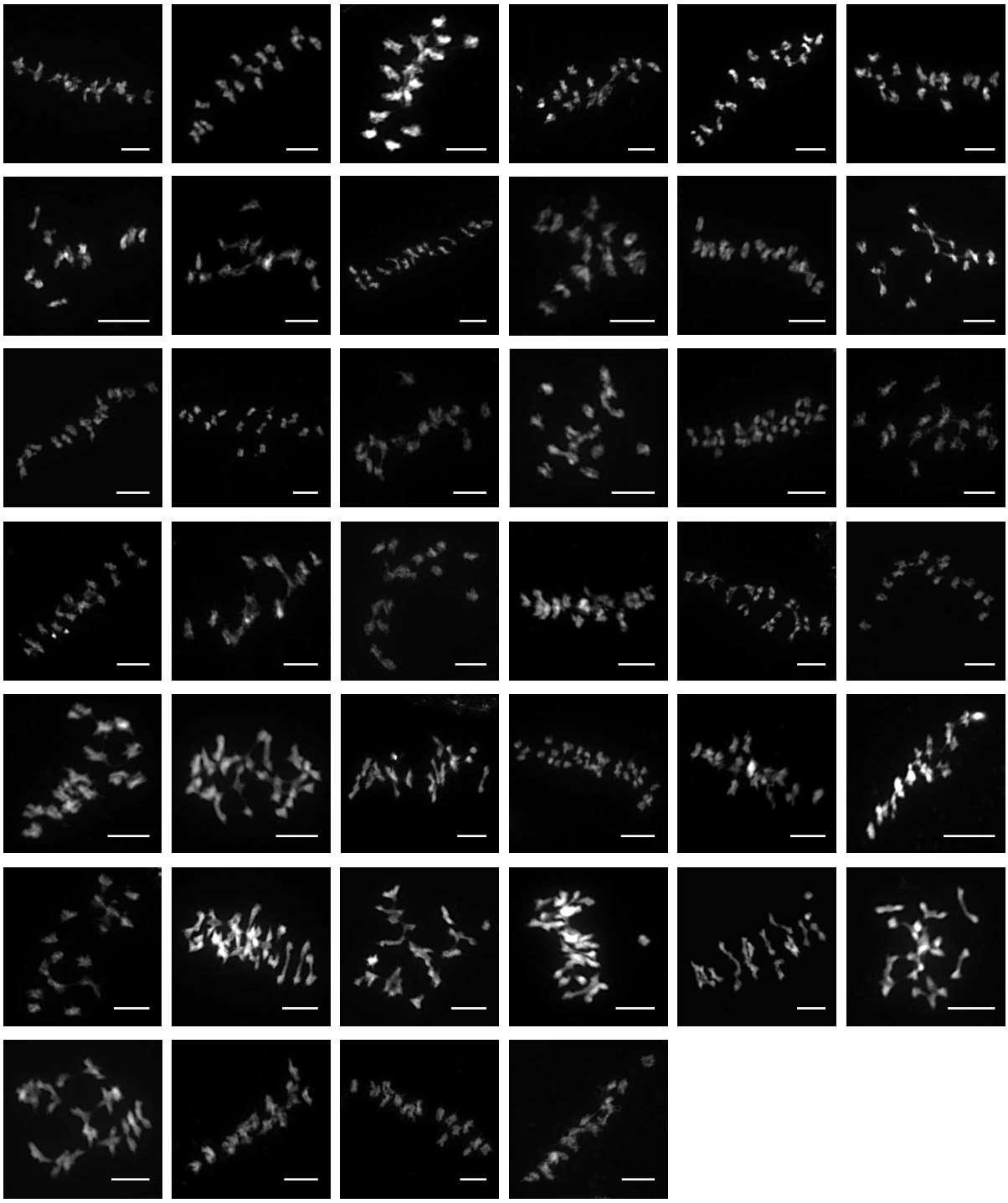

PIC9

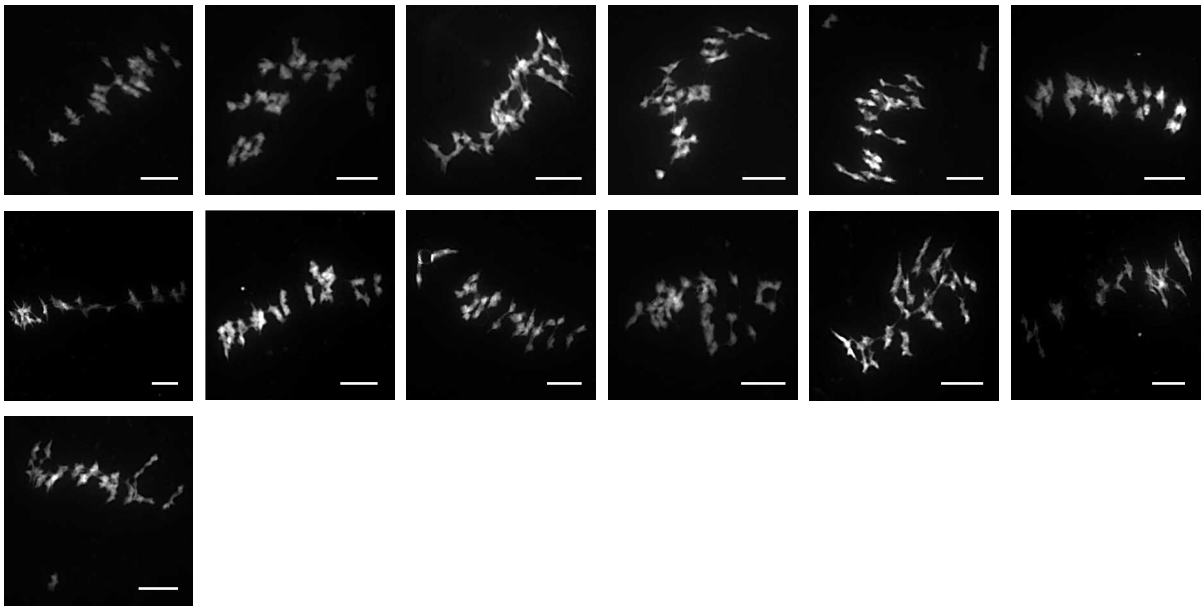

PIC11

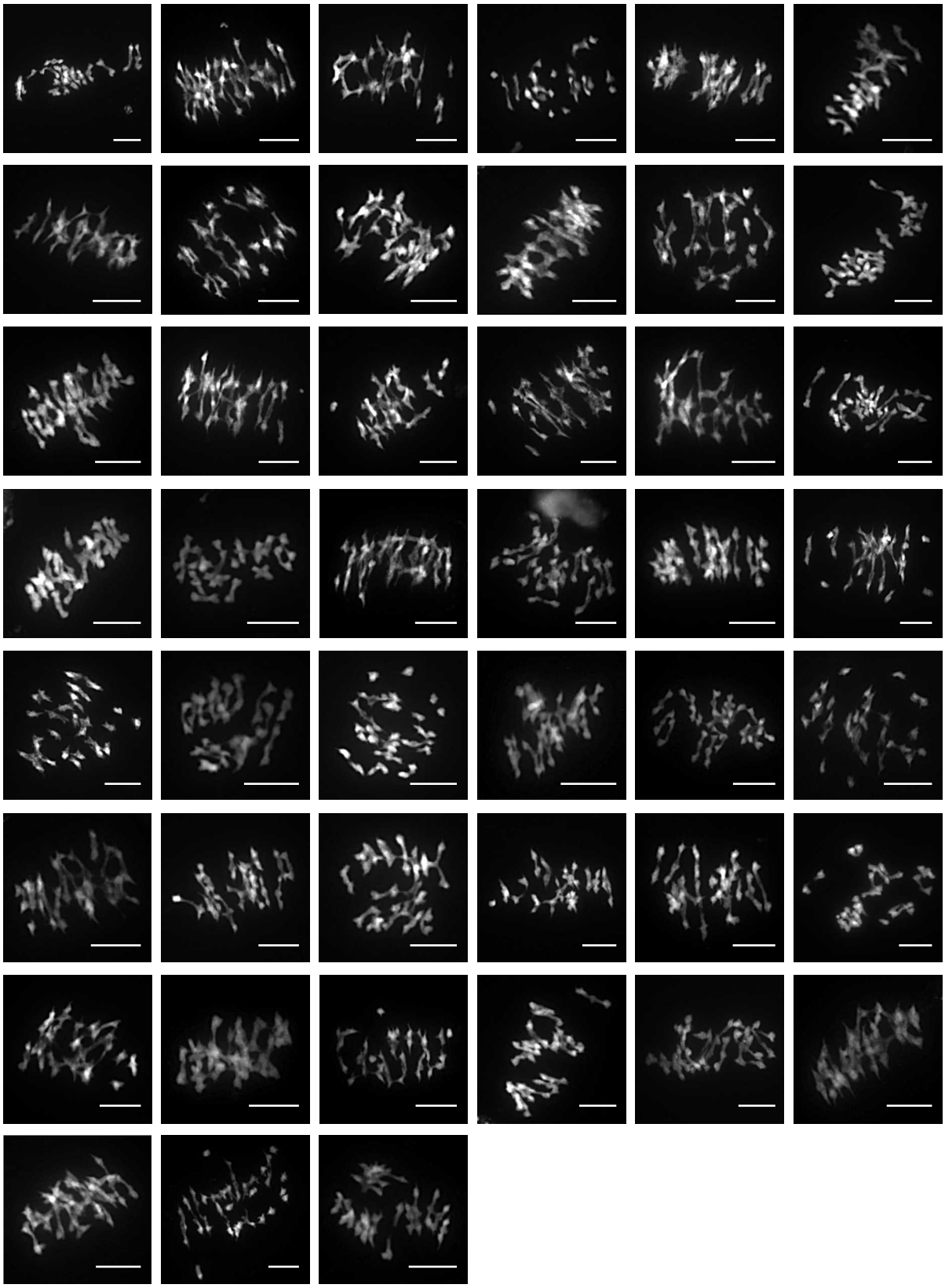

PIC14

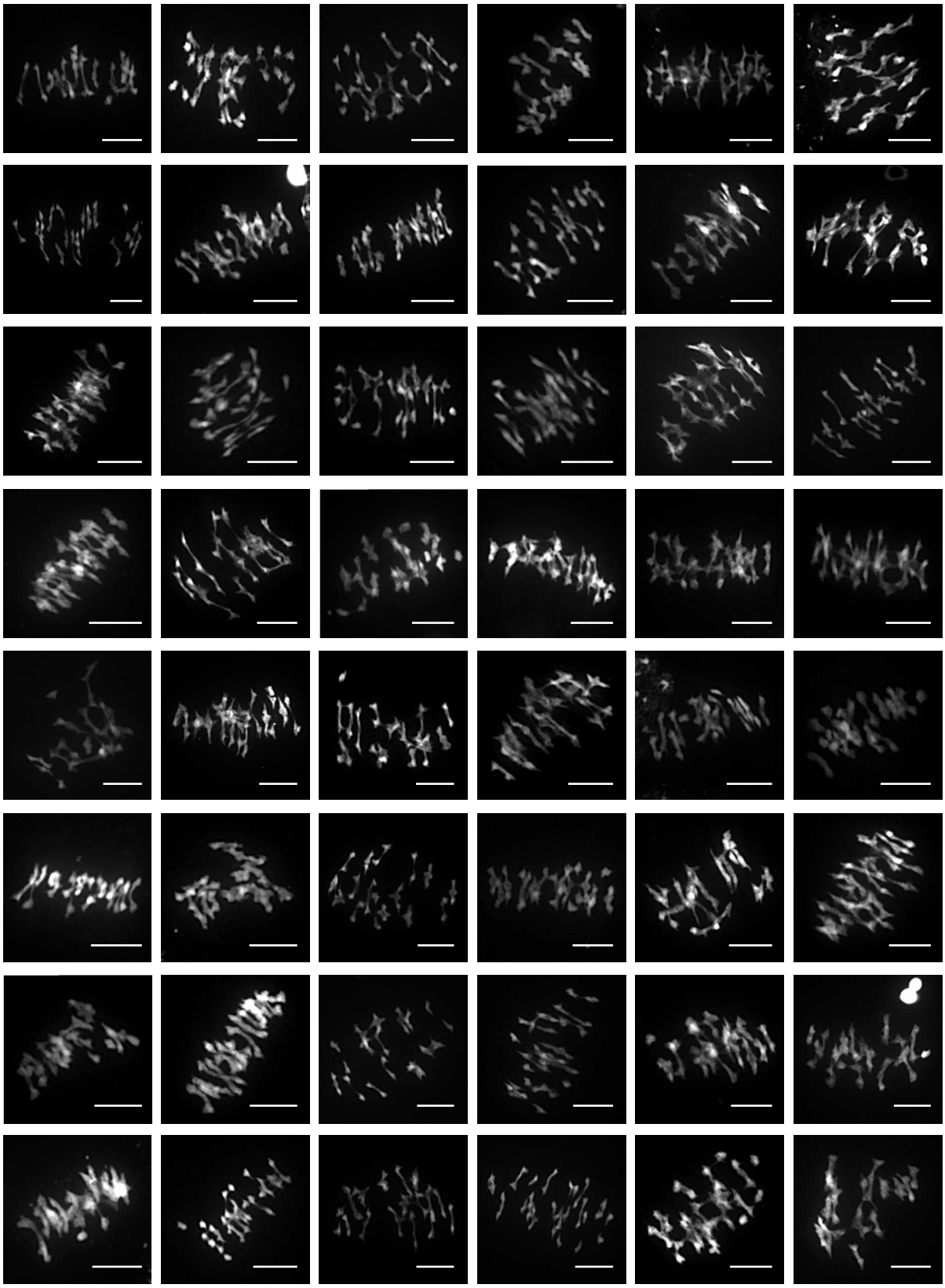

PIC14 (cont.)

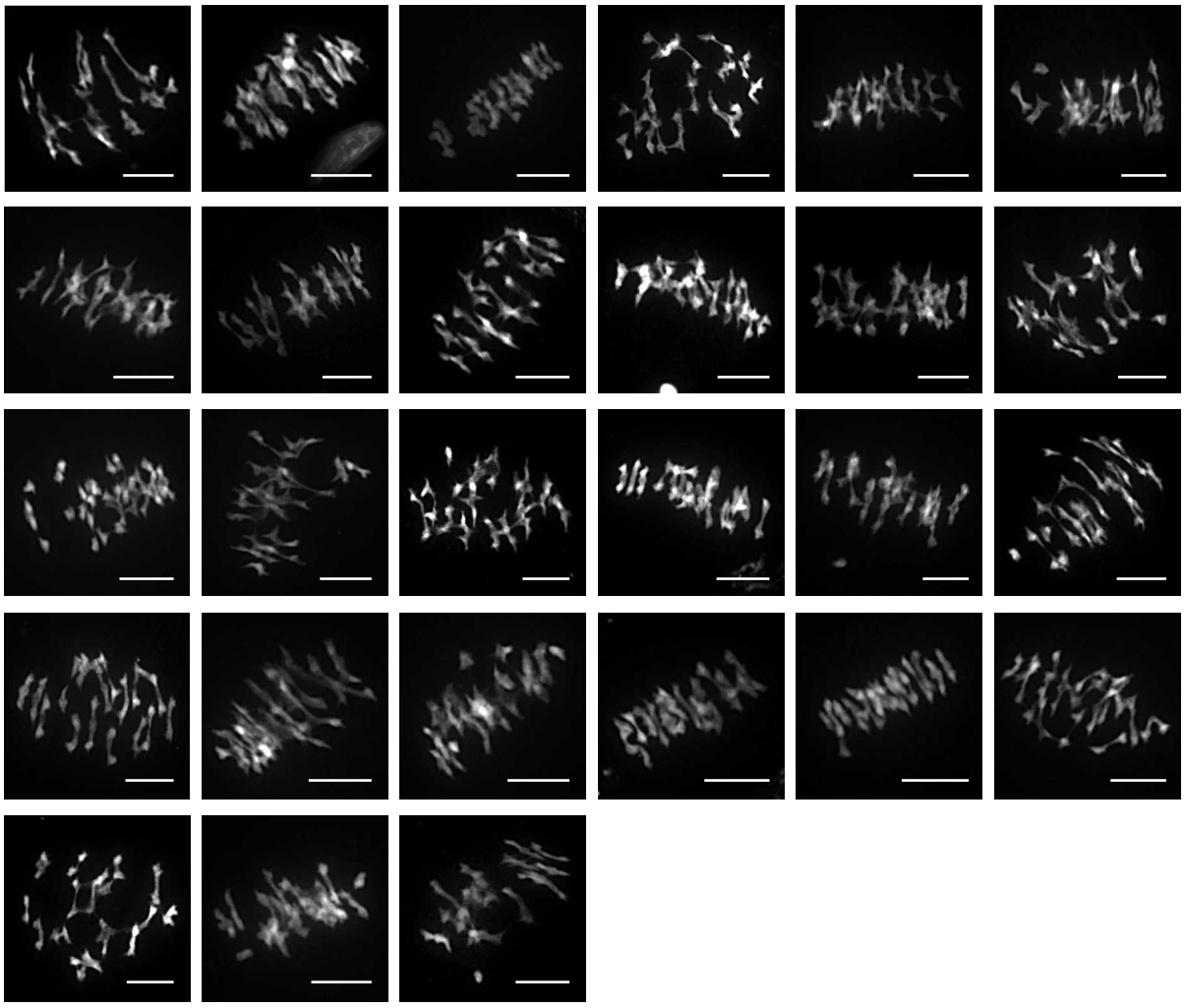

PIC18

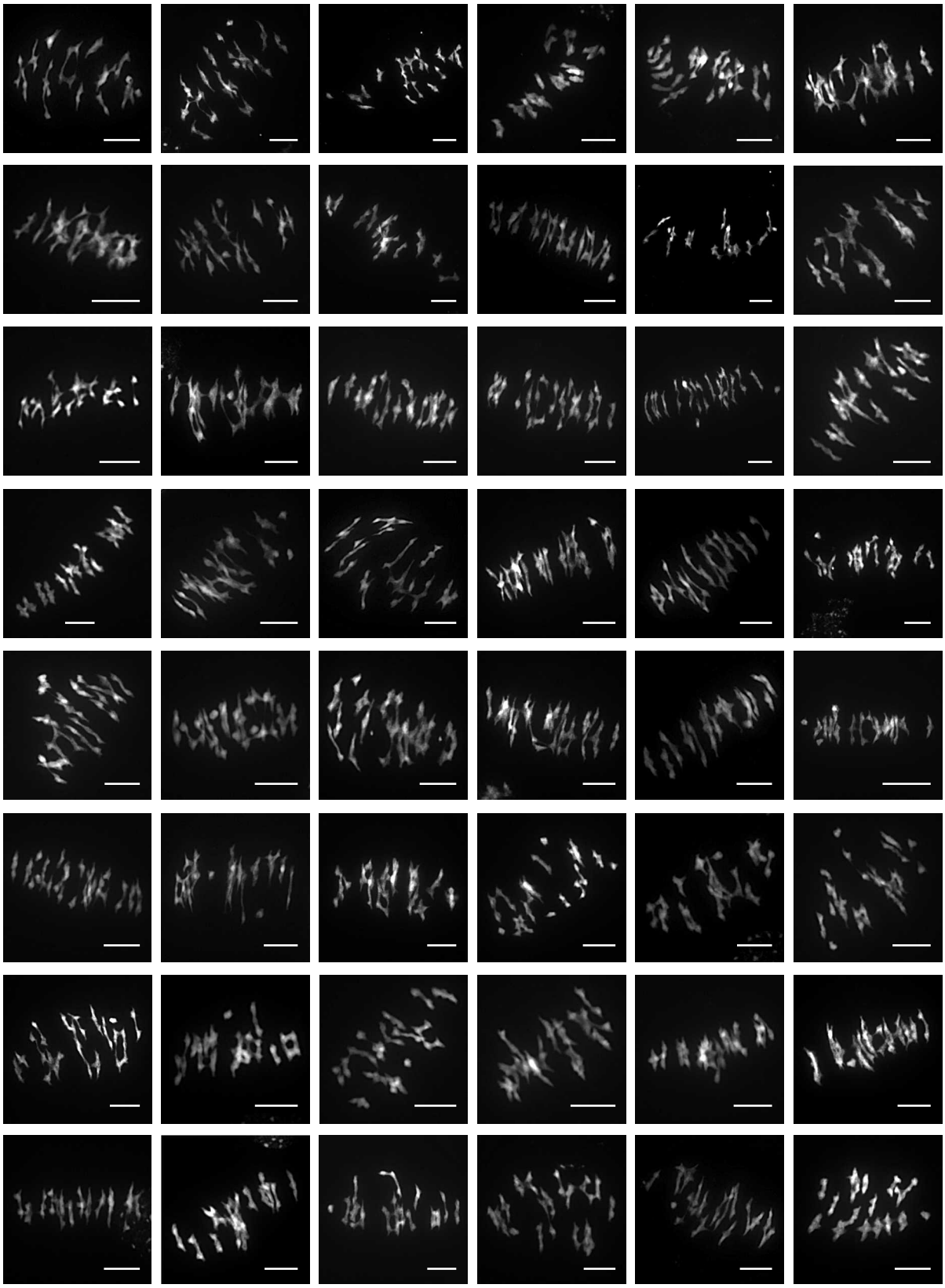

PIC18 (cont.)

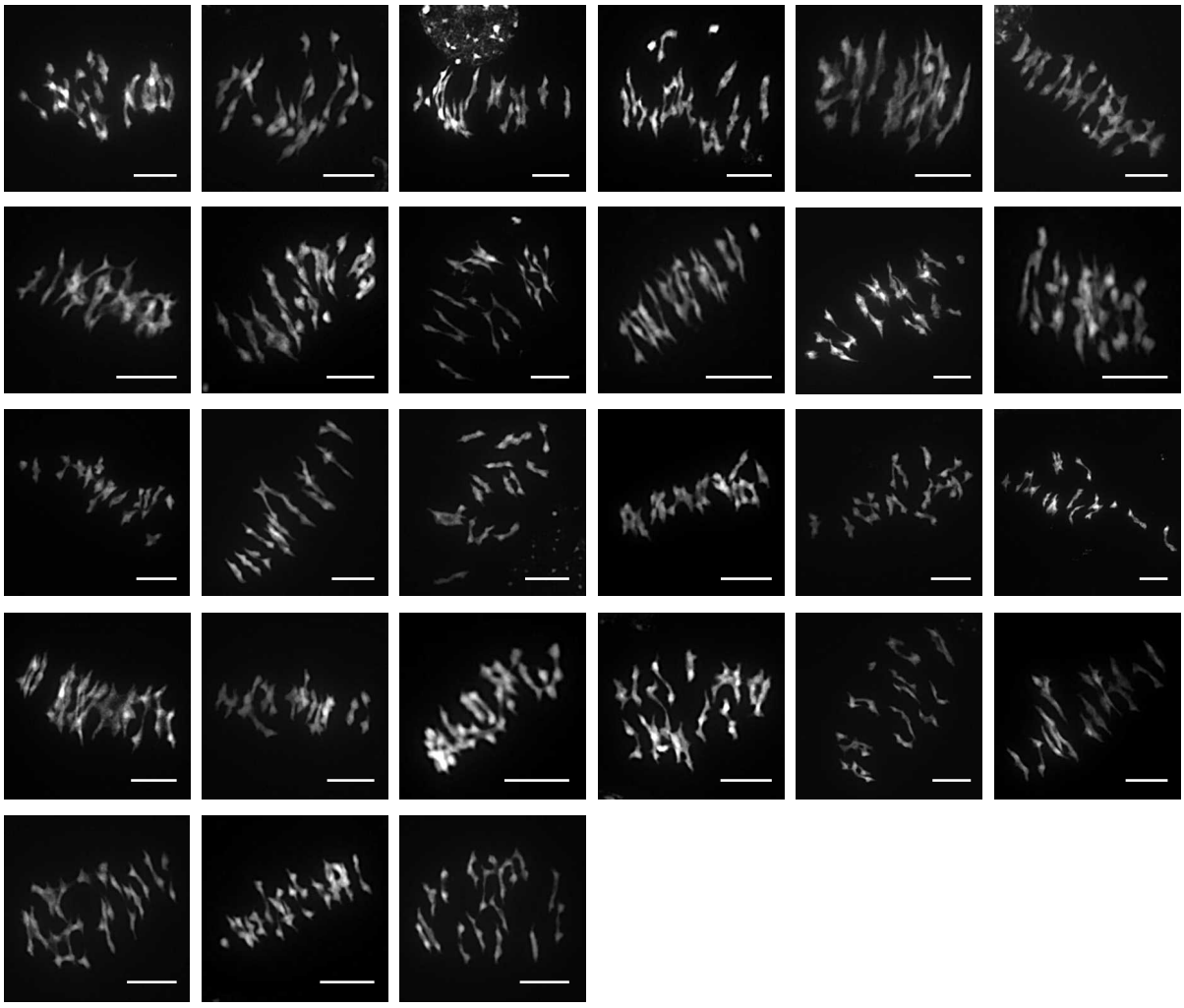

Other supplementary material

Additional data Tables (separate files)

Table S1. GPS coordinates of population localities.

Table S2. Mean depth of coverage (MDOC) per pool of individuals from each population.

Table S3. Genes in the top 1% of Fst scores (1000 bp windows) in C. amara. Note: red lines denote six genes which are candidates also in A. arenosa.

Table S4. GO terms enriched in C. amara WGD candidate genes. Annotated: # genes in the GO category, Significant: # candidate genes in each category, p-values crom Fisher's exact test ('elim' method).

Table S5. Top 1% of amino acid substitutions with the highest fineMAV score.

Table S6. Genes in the top 1% of Fst scores (1000 bp windows) in A. arenosa.

Table S7. GO terms enriched in A. arenosa WGD candidate genes. Annotated: # genes in the GO category, Significant: # candidate genes in each category, p-values crom Fisher's exact test ('elim' method).

Table S8. Targeted search for patterns suggesting directional selection in C. amara orthologs of candidate A. arenosa meiosis genes.

Table S9. Chromosome stability scoring of individual diploid (2n = 16) and autotetraploid (2n = 32) plants of *Cardamine amara* at meiotic metaphase I.

Table S10. *C. amara* candidate genes that have more than one associated protein among *A. arenosa* candidates.

Table S11. Quality checks of DNA isolated from LUZ.

Table S12. Assessment of genome completeness using BUSCO.